

# Far-red fluorescent genetically encoded calcium ion indicators

Received: 4 February 2022

Accepted: 24 March 2025

Published online: 07 April 2025

 Check for updates

Rochelin Dalangin<sup>1,2</sup>, Bill Z. Jia<sup>3,4</sup>, Yitong Qi<sup>3</sup>, Abhi Aggarwal<sup>5,6</sup>, Kenryo Sakoi<sup>7</sup>, Mikhail Drobizhev<sup>8,9</sup>, Rosana S. Molina<sup>8</sup>, Ronak Patel<sup>5</sup>, Ahmed S. Abdelfattah<sup>5,10</sup>, Jihong Zheng<sup>5</sup>, Daniel Reep<sup>5</sup>, Jeremy P. Hasseman<sup>5</sup>, The GENIE Project Team\*, Yufeng Zhao<sup>1,11</sup>, Jiahui Wu<sup>1,12</sup>, Kaspar Podgorski<sup>5,13</sup>, Alison G. Tebo<sup>5</sup>, Eric R. Schreiter<sup>5</sup>, Thomas E. Hughes<sup>8,14</sup>, Takuya Terai<sup>7</sup>, Marie-Eve Paquet<sup>2,15,16</sup>, Sean G. Megason<sup>4</sup>, Adam E. Cohen<sup>3</sup>, Yi Shen<sup>1</sup>✉ & Robert E. Campbell<sup>1,2,7,16</sup>✉

Genetically encoded calcium ion ( $\text{Ca}^{2+}$ ) indicators (GECIs) are widely-used molecular tools for functional imaging of  $\text{Ca}^{2+}$  dynamics and neuronal activities with single-cell resolution. Here we report the design and development of two far-red fluorescent GECIs, FR-GECO1a and FR-GECO1c, based on the monomeric far-red fluorescent proteins mKelly1 and mKelly2. FR-GECOs have excitation and emission maxima at ~596 nm and ~644 nm, respectively, display large responses to  $\text{Ca}^{2+}$  in vitro ( $\Delta F/F_0 = 6$  for FR-GECO1a, 18 for FR-GECO1c), are bright under both one-photon and two-photon illumination, and have high affinities (apparent  $K_d = 29$  nM for FR-GECO1a, 83 nM for FR-GECO1c) for  $\text{Ca}^{2+}$ . FR-GECOs offer sensitive and fast detection of single action potentials in neurons, and enable in vivo all-optical manipulation and measurement of cellular activities in combination with optogenetic actuators.

A property of most mammalian tissues is that they are most transparent to wavelengths of light between ~600 nm and ~1300 nm, a range often referred to as the optical window<sup>1,2</sup>. This wavelength range falls between the absorbance profile of hemoglobin, which predominates at wavelengths below ~600 nm, and the absorbance profile of water, which predominates at wavelengths longer than ~1300 nm. Due to the greater tissue transparency in this wavelength range, fluorescent probes that absorb and emit efficiently within the optical

window are desirable for in vivo imaging. In addition, fluorescent probes with longer excitation wavelengths are associated with lower phototoxicity and autofluorescence, reduced crosstalk with green fluorescent indicators, and better spectral compatibility with blue or cyan light-activated optogenetics tools.

In efforts to realize the advantages of fluorophores that excite and emit within the optical window, molecular tool engineers strive to shift the excitation and emission wavelengths of genetically encodable

<sup>1</sup>Department of Chemistry, University of Alberta, Edmonton, AB, Canada. <sup>2</sup>Centre de recherche CERVO, Québec, QC, Canada. <sup>3</sup>Department of Chemistry and Chemical Biology, Harvard University, Cambridge, MA, USA. <sup>4</sup>Department of Systems Biology, Harvard Medical School, Boston, MA, USA. <sup>5</sup>Janelia Research Campus, Howard Hughes Medical Institute, Ashburn, VA, USA. <sup>6</sup>Cumming School of Medicine, University of Calgary, and Hotchkiss Brain Institute, Calgary, Alberta, Canada. <sup>7</sup>Department of Chemistry, The University of Tokyo, Tokyo, Japan. <sup>8</sup>Department of Cell Biology & Neuroscience, Montana State University, Bozeman, MT, USA. <sup>9</sup>Department of Microbiology & Cell Biology, Montana State University, Bozeman, MT, USA. <sup>10</sup>Department of Neuroscience, and Carney Institute for Brain Science, Brown University, Providence, RI, USA. <sup>11</sup>Centre for Research and Applications in Fluidic Technologies, National Research Council of Canada, and Leslie Dan Faculty of Pharmacy, University of Toronto, Toronto, ON, Canada. <sup>12</sup>Department of Chemistry, University of Massachusetts, Amherst, MA, USA. <sup>13</sup>Allen Institute for Neural Dynamics, Seattle, WA, USA. <sup>14</sup>Montana Molecular, Bozeman, MT, USA. <sup>15</sup>Département d'anesthésiologie et soins intensifs, Université Laval, Québec, QC, Canada. <sup>16</sup>Département de biochimie, de microbiologie et de bio-informatique, Université Laval, Québec, QC, Canada.\*A list of authors and their affiliations appears at the end of the paper. ✉e-mail: [yi.shen@ualberta.ca](mailto:yi.shen@ualberta.ca); [campbell@chem.s.u-tokyo.ac.jp](mailto:campbell@chem.s.u-tokyo.ac.jp)

fluorescent proteins (FPs), such as standard red FPs (RFPs) with excitation maxima ( $\lambda_{ex}$ ) at 550 to 580 nm and emission ( $\lambda_{em}$ ) at 580 to 620 nm, into the far-red region of the spectrum. This longstanding effort has yielded a plethora of far-red FPs (Fig. 1A) with  $\lambda_{ex} > 580$  nm and  $\lambda_{em} > 620$  nm<sup>3–12</sup>. Efforts to engineer biliverdin (BV)-binding FPs, that fluoresce at even further red-shifted wavelengths, have resulted in near-infrared (NIR) FPs with  $\lambda_{ex} > 640$  nm and  $\lambda_{em} > 670$  nm<sup>13–15</sup>. The key difference between these two classes of genetically encodable fluorophores is that the red and far-red FPs autocatalytically form their own chromophore and are homologs of the green FP (GFP), but genetically encoded NIR FPs use the biliverdin cofactor as their chromophore.

Genetically encoded fluorophores can be engineered into genetically encoded indicators (also known as biosensors). One of the most important examples of these indicators is the family of genetically encoded Ca<sup>2+</sup> indicators (GECIs), which can be used for the real-time detection and imaging of cell signaling and neuronal activities. The latest generation of red GECIs for neuronal activity detection

includes jRCaMP1a,b, jRGECO1a, K-GECO1, and XCaMP-R, all with single-photon excitation and emission peaks outside of the optical window<sup>16–18</sup>. Among currently available RFP-based GECIs, the most red-shifted variant that uses an FP with an autocatalytic chromophore is CAR-GECO1 ( $\lambda_{ex}$  - 560 nm,  $\lambda_{em}$  - 609 nm)<sup>19</sup>. The recently reported near-infrared (NIR) GECI series, NIR-GECO1,2, is based on the BV-binding FP mFP<sup>20,21</sup>. NIR-GECO variants have excitation and emission peaks at 678 and 704 nm, respectively, with a 10-fold inverted response in fluorescence intensity upon Ca<sup>2+</sup> addition. Although the spectra of NIR-GECO1,2 lie well within the optical window, the molecular brightness of the NIR-GECO1,2 variants is relatively dim compared to RFP-based GECIs<sup>20,21</sup>. A GECI based on Förster resonance energy transfer (FRET) from a blue-shifted BV-binding FP to a red-shifted BV-binding FP, designated iGECI, provides higher brightness but smaller Ca<sup>2+</sup>-dependent changes in fluorescence<sup>22,23</sup>.

In an effort to achieve the ideal combination of red-shifted excitation and emission maxima and fluorescent brightness, we now report

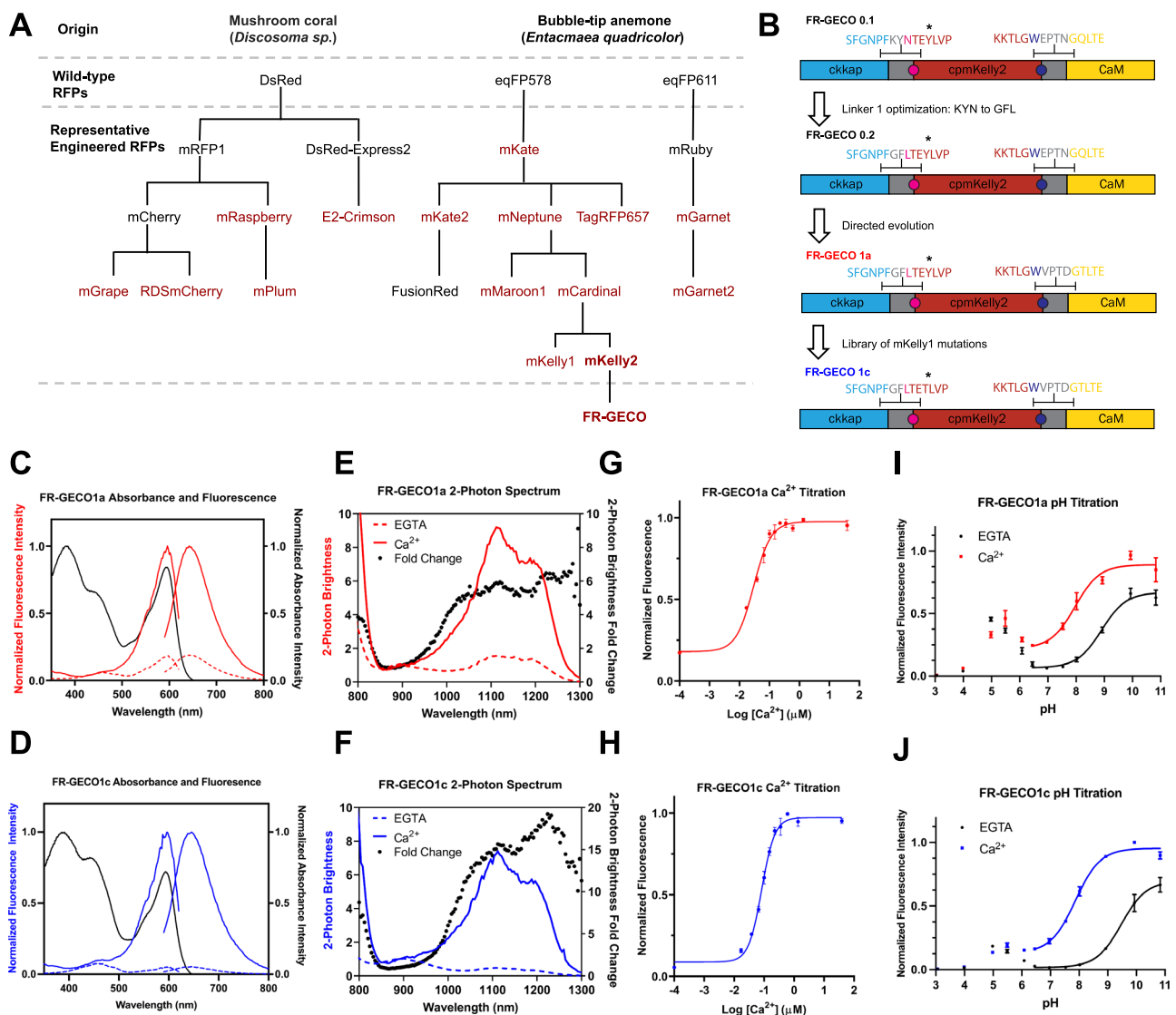


**Fig. 1 | Engineering and characterization of FR-GECO1a and FR-GECO1c.**

**A** Selected far-red FPs and FR-GECO genealogy. Far-red FPs ( $\lambda_{em} > 620$  nm) are highlighted in red. **B** Schematic illustration of FR-GECO1 design and engineering. Linker residues are in grey; asterisk indicates position 35. Magenta and blue-colored amino acids (and correspondingly colored circles in the schematic) represent the positions of ‘gatepost’ residues<sup>28</sup> that define the gatepost residues of cpmKelly2. Abbreviations: Calmodulin (CaM); CaM-dependent kinase kinase CaMKK- $\alpha/\beta$

peptide (cckap). Absorbance, excitation, and emission spectra of FR-GECO1a (**C**) and FR-GECO1c (**D**) with dashed lines representing the fluorescence spectra of the Ca<sup>2+</sup>-free state and solid lines representing the spectra of the Ca<sup>2+</sup>-bound state. Two-photon spectra and dynamic range of FR-GECO1a (**E**) and FR-GECO1c (**F**).  $K_d$  titration ( $n = 3$  technical replicates) with FR-GECO1a (**G**) and FR-GECO1c (**H**). pH sensitivity ( $n = 3$  technical replicates) of FR-GECO1a (**I**) and FR-GECO1c (**J**). Error bars represent S.E.M. Source data are provided in a Source Data file.

**Table 1 | Photophysical characterization of FR-GECO1a, FR-GECO1c, and mKelly2. Source data are provided in the Source Data file**

Protein Name	FR-GECO1a	FR-GECO1c	mKelly2*
Excitation maxima $\lambda_{ex}$ (nm)	596	596	598
Emission maxima $\lambda_{em}$ (nm)	642	646	649
Ca <sup>2+</sup> -dependent $\Delta F/F_0$	5.8 ± 0.2	18.1 ± 0.4	n/a
$K_d$ (nM)	29	83	n/a
Apparent Hill coefficient ( $n_H$ )	1.49	1.98	n/a
Apparent $pK_a$ (Ca <sup>2+</sup> free)	8.92	9.47	5.6
Apparent $pK_a$ (Ca <sup>2+</sup> bound)	7.96	7.88	n/a
$k_{on}$ (M <sup>-1</sup> s <sup>-1</sup> )	9.98 × 10 <sup>5</sup>	5.31 × 10 <sup>6</sup>	n/a
$\tau_{on}$ ( $\mu$ s)	1.00	0.188	n/a
$k_{off}$ (s <sup>-1</sup> )	3.71	6.39	n/a
$\tau_{off}$ (ms)	269	156	n/a
Extinction Coefficient $\epsilon$ (M <sup>-1</sup> cm <sup>-1</sup> ) (Ca <sup>2+</sup> free)	5710	4850	43,000
Extinction Coefficient $\epsilon$ (M <sup>-1</sup> cm <sup>-1</sup> ) (Ca <sup>2+</sup> bound)	27,000	26,500	n/a
Quantum Yield $\Phi$ (Ca <sup>2+</sup> free)	0.19	0.077	0.18
Quantum Yield $\Phi$ (Ca <sup>2+</sup> bound)	0.34	0.35	n/a
Brightness $\epsilon \times \Phi$ (×1000) (Ca <sup>2+</sup> free)	1.1	0.34	7.7
Brightness $\epsilon \times \Phi$ (×1000) (Ca <sup>2+</sup> bound)	9.2	9.4	n/a
2P Brightness $F_2$ (GM), $\lambda_{max}$ in parentheses (Ca <sup>2+</sup> free)	1.6 (1112 nm)	0.48 (1108 nm)	n/d
2P Brightness $F_2$ (GM), $\lambda_{max}$ in parentheses (Ca <sup>2+</sup> bound)	9.2 (1112 nm)	7.4 (1112 nm)	n/d
$\Delta F/F_0$ (2P), $\lambda_{max}$ in parentheses	5.9 (1112 nm)	15.4 (1112 nm)	n/a

\*Values from Wannier et al.<sup>12</sup>. Errors represent S.E.M. n/a not applicable, n/d not determined.

the development of a series of intensimetric far-red fluorescent GECI variants. Specifically, we report FR-GECO1a ( $\lambda_{ex}$  - 596 nm,  $\lambda_{em}$  - 642 nm) and FR-GECO1c ( $\lambda_{ex}$  - 596 nm,  $\lambda_{em}$  - 646 nm), which are based on the recently engineered far-red FPs mKelly1 ( $\lambda_{ex}$  - 596 nm,  $\lambda_{em}$  - 656 nm) and mKelly2 ( $\lambda_{ex}$  - 598 nm,  $\lambda_{em}$  - 649 nm)<sup>12</sup>. These far-red GECIs open avenues for multicolor Ca<sup>2+</sup> imaging in combination with other optogenetic indicators and actuators, as well as deeper tissue in vivo Ca<sup>2+</sup> imaging.

## Results

### Protein engineering

Initial efforts to engineer a far-red Ca<sup>2+</sup> indicator followed two parallel strategies. The first strategy was to graft key mutations for far-red fluorescence onto existing red GECIs. We used R-GECO1<sup>24</sup>, CH-GECO1<sup>25</sup> and K-GECO1<sup>17</sup> as templates and introduced key mutations from E2-Crimson ( $\lambda_{ex}$  - 611 nm,  $\lambda_{em}$  - 646 nm, tetrameric)<sup>5</sup>, RDSmCherry ( $\lambda_{ex}$  - 600 nm,  $\lambda_{em}$  - 630 nm)<sup>10</sup>, and mNeptune ( $\lambda_{ex}$  - 600 nm,  $\lambda_{em}$  - 650 nm)<sup>4</sup>, respectively (Fig. 1A, Supplementary Table 1). Unfortunately, the resulting prototypes showed complete loss of fluorescence or no substantial spectral red-shifts. The second strategy was de novo engineering of a GECI starting from far-red FP scaffolds. However, our initial attempts to engineer GECI based on mNeptune<sup>4</sup> and mCardinal<sup>6</sup> did not yield fluorescent prototypes. As both mNeptune and mCardinal retained weak dimerization tendencies<sup>4,6,12,26</sup>, we suspected that the failure of these prototypes to fluoresce could be due to overlap between the circular permutation site and/or insertion site of calmodulin and its binding peptide with the oligomerization interface, possibly disrupting dimerization that was crucial to the proper folding and/or chromophore maturation of these proteins.

mKelly1 and mKelly2 are far-red FP variants of mCardinal that were engineered to have increased monomericity by a combination of a C-terminal tail deletion, directed evolution, and consensus design<sup>12</sup> (Fig. 1A). We reasoned that the enhanced monomericity of mKelly1 and mKelly2 might facilitate circular permutation and further engineering to create GECIs. K-GECO1 was chosen as the starting scaffold because the use of the ckkap peptide, instead of RS20 as the calmodulin binding peptide, contributes to this indicator having high sensitivity, high Ca<sup>2+</sup> affinity, good linearity between fluorescence and Ca<sup>2+</sup> concentration, and fast response kinetics<sup>17</sup>. More importantly, it is currently the only GECI engineered using an FP variant derived from eqFP578, from which mKelly2 was also derived (Fig. 1A). We thus replaced the circularly permuted (cp) FusionRed RFP portion of K-GECO1 with cpmKelly2 (Supplementary Fig. 1), the brighter of the two mKelly variants. Thr143 and Trp140 (numbering according to the structure for FusionRed; PDB ID: 6U1A)<sup>27</sup> are the gatepost residues of mKelly2, which flank the bulge that has been identified as the privileged site for inserting sensing domains by structural and mechanistic analysis of engineered single FP-based biosensors<sup>28</sup>. As in K-GECO1, the ckkap peptide was attached to the N-terminal gatepost residue (Thr143 in FusionRed; Thr32Asn in K-GECO1) by a Lys-Tyr linker and CaM was linked to the C-terminal gatepost residue (Trp140 in FusionRed; Trp262 in K-GECO1) by a Glu-Pro-Thr-Asn linker (Supplementary Fig. 1). The initial construct resulted in a dimly fluorescent variant we named FR-GECO0.1 (Fig. 1B). Optimization of linker1 (the amino acids linking the ckkap peptide to cpmKelly2) led to the identification of an improved, but still dim, variant, FR-GECO0.2, with  $\lambda_{ex}$  = 586 nm,  $\lambda_{em}$  = 632 nm and -7-fold increase of fluorescence upon Ca<sup>2+</sup> addition. We then subjected FR-GECO0.2 to eight rounds of iterative directed evolution to improve its brightness and Ca<sup>2+</sup> response while ensuring that all the variants chosen to be used as gene templates for the next round maintained a far-red emission peak (Fig. 1B). Ultimately, our efforts led to a bright and sensitive far-red GECI, FR-GECO1a, which incorporated 19 mutations relative to the initial FR-GECO0.1 (Supplementary Table 2). FR-GECO1a has  $\lambda_{ex}$  = 596 nm,  $\lambda_{em}$  = 642 nm, and exhibits a 6-fold increase in fluorescence intensity in the presence of Ca<sup>2+</sup> (Fig. 1C).

With the mKelly2-derived FR-GECO1a in hand, we attempted to incorporate mKelly1-specific mutations in an effort to achieve a slightly more red-shifted emission peak and higher photostability<sup>12</sup>. Notably, mKelly1 was engineered from mCardinal in parallel with mKelly2, and it differed from mKelly2 by six mutations. To test whether these mutations could further improve FR-GECO1a, we screened a combinatorial library of FR-GECO1a containing all possible combinations of the six mKelly1-specific mutations. From this library, we isolated a variant with  $\lambda_{ex}$  = 596 nm and  $\lambda_{em}$  = 646 nm. It also exhibited an 18-fold increase in fluorescence intensity in the Ca<sup>2+</sup>-bound state, which is an over 2-fold improvement relative to that of FR-GECO1a. This variant, which we named FR-GECO1c (c for contrast) incorporated a single mutation, Tyr35Thr (numbering according to FR-GECO1a sequence, Fig. 1B and Supplementary Fig. 1) which is positioned in close proximity to the first gatepost residue, Leu32 (Fig. 1B)<sup>28</sup>.

### In vitro characterization

To characterize the photophysical properties of FR-GECO1a and FR-GECO1c, we purified the bacterially-expressed protein. Spectral analysis of the purified proteins revealed that the 596 nm excitation peak of both FR-GECO1a and FR-GECO1c is slightly blue-shifted by 2 nm relative to mKelly2 (598 nm) and that the emission peaks of the FR-GECO1a (642 nm) and FR-GECO1c (644 nm) are also slightly blue-shifted relative to mKelly2 (649 nm) (Fig. 1C, D and Table 1). The one-photon (1P) molecular brightness of FR-GECO1a (9.2) and FR-GECO1c (9.4) in their Ca<sup>2+</sup>-bound states are approximately 20% brighter than their template FP, mKelly2 (7.7) (Table 1). These results are attributed to a near doubling of the quantum yield (QY or  $\Phi$ ), which offset the

effect of the indicators' smaller effective extinction coefficients (EC or  $\epsilon$ ) compared to mKelly2. In the  $\text{Ca}^{2+}$ -free and  $\text{Ca}^{2+}$ -bound states, FR-GECO1a has ECs of 5710 and 27,000  $\text{M}^{-1}\text{cm}^{-1}$ , respectively, and FR-GECO1c has ECs of 4850 and 26,500  $\text{M}^{-1}\text{cm}^{-1}$ . The twofold increase in the  $\text{Ca}^{2+}$ -dependent  $\Delta F/F_0$  of FR-GECO1c relative to FR-GECO1a (attributable to the Tyr35Thr mutation), was found to result primarily from the two-fold smaller QY in the  $\text{Ca}^{2+}$ -free state of FR-GECO1c. Under two-photon (2P) conditions, both FR-GECO1a and FR-GECO1c have peak 2P excitation at 1112 nm (Fig. 1E, F), with FR-GECO1a having a ~25% higher 2P molecular brightness (9.2 GM) than FR-GECO1c (7.4 GM) in the  $\text{Ca}^{2+}$ -bound state (Table 1). Both FR-GECO1a and FR-GECO1c, in  $\text{Ca}^{2+}$ -saturated states in vitro, are among the brightest red GECIs upon 2P excitation<sup>29</sup> (Supplementary Table 3). The optimal wavelength range for 2P excitation, with close to maximum fluorescence change, was between 1050 and 1200 nm (Fig. 1E, F). The overall  $\Delta F/F_0$  of FR-GECO1a and FR-GECO1c under 1P and 2P conditions are comparable. Taken together, FR-GECO1a and FR-GECO1c exhibit bright far-red fluorescence under both 1P and 2P illumination.

Consistent with other cckap-based GECIs<sup>17,18,30</sup>, static  $\text{Ca}^{2+}$  titrations revealed that both FR-GECO1a and FR-GECO1c have relatively high affinities for  $\text{Ca}^{2+}$  and Hill coefficients ( $n_H$ ) greater than unity (Fig. 1G, H). FR-GECO1a ( $K_d = 32$  nM;  $n_H = 1.49$ ) has a substantially lower  $K_d$  and  $n_H$  than FR-GECO1c ( $K_d = 87$  nM;  $n_H = 1.98$ ). These relatively high  $\text{Ca}^{2+}$  binding affinities suggested FR-GECO1a and FR-GECO1c would be well-suited for neuronal activity detection. Kinetic measurements revealed fast fluorescence responses from  $\text{Ca}^{2+}$  association and dissociation for both FR-GECO1a and FR-GECO1c (Table 1, Supplementary Fig. 2). Specifically, FR-GECO1a ( $\tau_{\text{off}} = 269$  ms) and FR-GECO1c ( $\tau_{\text{off}} = 156$  ms) are among the fastest decaying GECIs with high  $\text{Ca}^{2+}$  affinity<sup>31</sup>. The pH dependence (Fig. 1I, J) indicated that both FR-GECO1 variants undergo a shift in  $\text{pK}_a$  upon binding  $\text{Ca}^{2+}$  with a  $\text{pK}_a$  of -9 in the  $\text{Ca}^{2+}$ -free state and -8 in the  $\text{Ca}^{2+}$ -bound state. Both variants exhibited a small peak at pH = 5 in the  $\text{Ca}^{2+}$ -free state and 5.5 in the bound state, suggesting multiple ionizable groups, as previously observed for the pH profile of the CH-GECO series of red GECIs<sup>32</sup>. In cultured HeLa cells, both FR-GECO1 variants gave robust responses to histamine-induced  $\text{Ca}^{2+}$  oscillations, with an average maximum  $\Delta F/F_0$  value of  $4.1 \pm 0.3$  for FR-GECO1c and  $1.1 \pm 0.06$  for FR-GECO1a. In response to complete depletion and saturation of  $\text{Ca}^{2+}$  (with EGTA/ionomycin and  $\text{Ca}^{2+}$ /ionomycin, respectively), FR-GECO1c gave an average  $\Delta F/F_0$  of  $10.4 \pm 1.0$  and FR-GECO1a gave an average  $\Delta F/F_0$  of  $2.8 \pm 0.2$  (Supplementary Fig. 3). These changes are about 50% of those observed with the purified proteins (Table 1).

To test whether FR-GECOs can be photoactivated by blue light (as observed for the R-GECO family of red GECIs and, to a lesser extent, K-GECO1<sup>16,17,19</sup>), purified proteins were imaged using 561 nm (3.70 W/cm<sup>2</sup>) excitation laser with 488 nm (0.71 W/cm<sup>2</sup>) blue light laser pulses (50 ms). FR-GECO1a and FR-GECO1c were found to exhibit moderate increases in far-red fluorescence emission with blue light illumination, in both the  $\text{Ca}^{2+}$ -bound and  $\text{Ca}^{2+}$ -free states (Supplementary Fig. 4). However, unlike R-GECO1 ( $t_{1/2} = 0.56$  s for  $\text{Ca}^{2+}$ -free state)<sup>33</sup>, the photoactivation rise and decay of FR-GECOs happens within 10 s of milliseconds.

### Performance in cultured neurons

The in vitro characterization of FR-GECO1a and FR-GECO1c revealed that, in addition to their red-shifted fluorescence spectra which enable efficient excitation at wavelengths ~596 nm (where jRGECO1a and jRCaMP1a are poorly excitable), these two GECIs had properties, such as large fluorescence changes and high  $\text{Ca}^{2+}$  affinities, comparable to state-of-the-art GECIs. Of the two indicators, we expected that FR-GECO1a may be more suitable for labeling fine subcellular neuronal processes, such as axons and dendrites, due to its brighter  $\text{Ca}^{2+}$ -free state as shown by the characterization in vitro. On the other hand, we expected that FR-GECO1c may provide better performance for the

detection of single spikes in neurons in terms of fluorescence change because of its larger  $\text{Ca}^{2+}$ -dependent  $\Delta F/F_0$  in vitro relative to FR-GECO1a. To evaluate the performance of FR-GECO1a and FR-GECO1c for imaging neuronal activity and compare them against jRGECO1a and jRCaMP1a, two state-of-the-art red GECIs, we expressed each GECI in dissociated rat hippocampal and cortical neurons. Similar to the red GECIs, we observed that the fluorescence in neurons expressing either FR-GECO1 variant was evenly distributed throughout the cytosol (Fig. 2A). Of the two indicators, FR-GECO1a did, indeed, have brighter basal fluorescence, providing easier identification of transfected cells as well as facilitating visualization of the fine morphology of neural cells (Fig. 2A, H).

To evaluate indicator functions, we acquired fluorescence images while delivering electric field stimuli to evoke action potentials (APs) (in trains of 3, 10, 160 APs). FR-GECO1a and FR-GECO1c showed  $\Delta F/F_0$  of 27% and 28%, respectively, upon 3 APs evoked by the field electrode, similar to jRGECO1a and jRCaMP1a, which showed  $\Delta F/F_0$  of 34% and 33%, respectively (Fig. 2B–D). When evoked with 160 stimuli, neurons expressing FR-GECO1a exhibited a  $\Delta F/F_0$  of 82% while FR-GECO1c had a  $\Delta F/F_0$  of 161% compared to 113% and 107% for jRGECO1a and jRCaMP1a, respectively (Fig. 2D). FR-GECO1a showed a slightly slower rise time than the other three sensors for 3 and 10 APs (half rise time, FR-GECO1a: 0.29 s for 3 AP and 0.32 s for 10 AP), but both FR-GECO1a and FR-GECO1c (half rise time, FR-GECO1a: 0.61 s for 160 AP and FR-GECO1c: 0.59 s) had ~1-fold larger half rise times than jRGECO1a (half rise time: 0.35 s) and jRCaMP1a (half rise time: 0.39 s) with 160 APs (Fig. 2E). Both indicators exhibited relatively fast decay (half decay time, FR-GECO1a: 0.78 s and 0.70 s; FR-GECO1c: 0.80 s and 0.41 s, for 3 and 10 APs, respectively) times comparable to, or faster than, jRGECO1a and jRCaMP1a (half decay time, jRGECO1a: 0.61 s and 0.51 s; jRCaMP1a: 0.52 s and 1.0 s, for 3 and 10 APs, respectively) (Fig. 2F). Of the sensors tested, jRCaMP1a was most notable for its slower decay time (Fig. 2B, C, F). Relative to jRGECO1a and jRCaMP1a, FR-GECO1c exhibited a similar signal-to-noise ratio (SNR) and FR-GECO1a exhibited modestly lower SNR (Fig. 2G). Both FR-GECO1 variants provided robust responses to spontaneous activity in cortical neurons (Supplementary Fig. 5). Overall, these results suggest that both FR-GECO1a and FR-GECO1c enable sensitive detection of neuronal activities. FR-GECO1c, in particular, offers good response times, and large fluorescence changes, comparable to other state-of-art red GECIs<sup>16–18</sup>.

### $\text{Ca}^{2+}$ optopatch for all-optical cardiac electrophysiology in vivo in zebrafish embryonic heart

To investigate how FR-GECO1 performs in zebrafish, we compared its performance to state-of-the-art near-infrared GECIs based on BV-dependent FPs. In the spontaneously beating linear heart tubes (LHTs) of 1 day-old embryos, FR-GECO1 showed significantly larger  $\text{Ca}^{2+}$ -dependent changes in fluorescence ( $\Delta F/F_0 = 11\%$  for FR-GECO1a and 30% for FR-GECO1c) than NIR-GECO2 ( $\Delta F/F_0 = 3\%$ ) and NIR-GECO2G ( $\Delta F/F_0 = 3\%$ ) (Fig. 3A, B). In our hands, iGECI expressed in the zebrafish heart (Fig. 3C) did not show detectable fluorescence transients in the range of frequencies expected for cardiac calcium dynamics (Fig. 3A, D; Methods). Similar to what we observed during the in vitro characterization, FR-GECO1a had a stronger mean intensity (intensity = 170 arbitrary units (AU)) than FR-GECO1c (intensity = 50 AU) and comparable fluorescence intensities with the other near-infrared GECIs tested (intensity = 200 AU for NIR-GECO2, 120 AU for NIR-GECO2G and 250 AU for iGECI; Fig. 3C). Regardless, both FR-GECO1 variants had significantly larger SNR (FR-GECO1a: 140; FR-GECO1c: 230) than the near-infrared GECIs (SNR, NIR-GECO2: 13; NIR-GECO2G: 15; iGECI: 1.8; Fig. 3D). Exogenous addition of BV did not lead to significant improvements in performance for FR-GECO and the near-infrared GECIs (Supplementary Fig. 6).

Spectrally compatible combinations of channelrhodopsins and GECIs (that is, a  $\text{Ca}^{2+}$  optopatch system) can enable the simultaneous

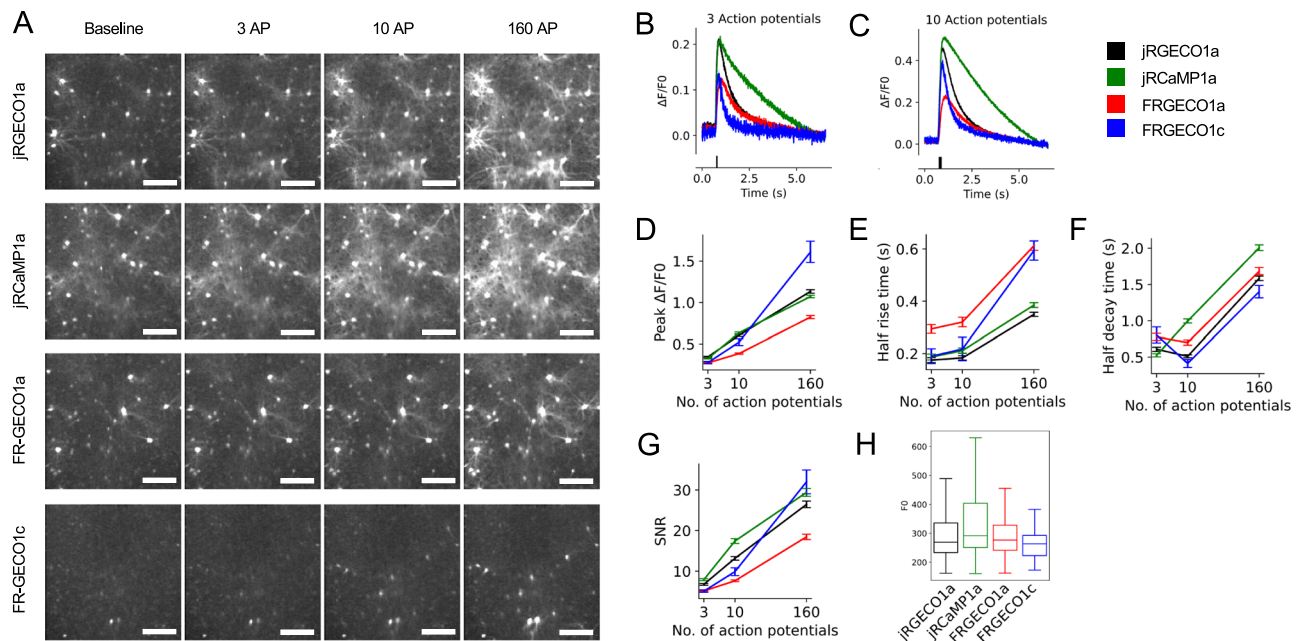


**Fig. 2 | Performance of FR-GECO1 variants in cultured neurons. A** Representative images of neurons expressing jRGECO1a (repeated in 96 wells over 8 plates), jRCaMP1a (repeated in 77 wells over 8 plates), FR-GECO1a (repeated in 58 wells over 5 plates), FR-GECO1c (repeated in 47 wells over 5 plates), at baseline, and stimulation with 3 action potentials (AP), 10 action potentials, and 160 action potentials. All repeats gave similar results. Scale bar is 200  $\mu\text{m}$  in all images. **B, C** Fluorescence response as a function of time following 3 action potentials (**B**) and 10 action potentials (**C**). Fluorescence responses (**D**), half rise time (**E**), half decay time (**F**), SNR (**G**), and basal fluorescence (**H**), of jRGECO1a (black;  $n = 1482$  cells), jRCaMP1a

(green;  $n = 1043$  cells), FR-GECO1a (red;  $n = 601$  cells), and FR-GECO1c (blue;  $n = 171$  cells). Colors are consistent throughout the figure. All indicators were excited with 565 nm LED and imaged with mCherry filter cubes (excitation 560/40 nm, dichroic mirror 585LP and emission 630/75 nm). For **D–G**, error bars represent S.E.M. For **H**, the box indicates the 25th to 75th percentile range, the horizontal line indicates the median, and the whiskers extend from the box to the farthest data point lying within  $1.5 \times$  the inter-quartile range (IQR). Data points beyond the boundary of the higher whisker were removed.

all-optical manipulation and measurement of neural activities across large populations of neurons at a cellular, or even subcellular, resolution. However, the spectral overlap between many of the blue light-activated optogenetic actuators and many of the existing red GECIs based on GFP-like FPs has posed a major hurdle for developing such systems. Specifically, blue light illumination can induce transient increases in red GECI fluorescence<sup>16</sup> and the red-shifted GECI excitation light can induce channelrhodopsin photocurrents. Currently, maximum spectral separation is achieved with near-infrared GECIs based on BV-binding FPs, which limits their application in physiological contexts with low BV bioavailability. However, the particularly red-shifted fluorescence excitation spectrum of FR-GECO1a,c presents an opportunity to minimize optical crosstalk with blue light-activated channelrhodopsins such as CheRiff, a fast and sensitive blue-shifted channelrhodopsin with a peak  $\lambda_{\text{ex}}$  of  $\sim 460$  nm<sup>34</sup>.

Having verified that FR-GECO1 performs well in zebrafish, we then proceeded to examine the spectral orthogonality between FR-GECO and CheRiff. First, we characterized the blue light activation of FR-GECO1a,c in cultured neuron cells. High intensity 470 nm blue light (23 mW/mm<sup>2</sup>) illumination only induced a moderate transient increase ( $\Delta F/F_0 \leq 0.1$ ) in far-red fluorescence intensity. In accordance with our in vitro characterization with purified proteins, FR-GECO1a,c fluorescence returned to pre-activation baseline level in  $<10$  ms after removal of blue light illumination (Fig. 4A). We then evaluated the photocurrent of CheRiff during illumination with 594 nm light. Typical photocurrents induced by 594 nm light at imaging intensities were between 2–4% of the maximum blue light-induced photocurrent, and are therefore unlikely to trigger spurious action potentials (Fig. 4B).

Having demonstrated this minimal optical crosstalk, we proceeded to co-express FR-GECO and CheRiff in cultured neurons. Activation of CheRiff with 470 nm blue light produced Ca<sup>2+</sup> transients that were reliably reported by both FR-GECO1a and FR-GECO1c under

excitation at 594 nm. CheRiff stimulation with 0.6 s of 470 nm light (0.07 mW/mm<sup>2</sup>) resulted in  $\Delta F/F_0$  values of 20% and 60% for FR-GECO1a and FR-GECO1c, respectively (Fig. 4C). When activation light intensity was increased to 0.35 mW/mm<sup>2</sup>, FR-GECO1a and FR-GECO1c exhibited  $\Delta F/F_0$  values of 100% and 280%, respectively (Fig. 4D). Collectively, these results indicate that, due to their red-shifted spectra, FR-GECO1a and FR-GECO1c are well-suited for multiplexing with the blue-light activated optogenetic actuator CheRiff.

Following the determination of the spectral orthogonality between FR-GECO and CheRiff in cultured cells and the comparison between FR-GECO and available near-infrared GECIs in zebrafish, we further evaluated this Ca<sup>2+</sup> optopatch system in vivo in zebrafish. Previous work has shown that activation of channelrhodopsins expressed in sinoatrial cardiomyocytes can trigger heartbeats<sup>35</sup>. In the heart, Ca<sup>2+</sup> influx is involved in action potential generation, and Ca<sup>2+</sup>-triggered Ca<sup>2+</sup> release from the sarcoplasmic reticulum is involved in triggering muscle contraction. Embryonic zebrafish expressing only FR-GECO1c exhibited an average  $\Delta F/F_0$  of 7% during rhythmic spontaneous Ca<sup>2+</sup> oscillations 24 h post-fertilization (hpf) in the zebrafish LHT (Fig. 4E, F Supplementary Movie 1). To simultaneously pace and measure the Ca<sup>2+</sup> dynamics in the LHT, both FR-GECO1a and CheRiff were expressed in zebrafish embryos. Optical stimulation of CheRiff using blue light (488 nm light at 24 mW/mm<sup>2</sup> and 1 Hz) induced reliable Ca<sup>2+</sup> transients that were reported by FR-GECO1a ( $\lambda_{\text{ex}} = 594$  nm; Fig. 4G). Similar results were observed with the combination of FR-GECO1a and CoChR<sup>36</sup>, another blue light-activated channelrhodopsin that is capable of generating large photocurrents and that has previously been used in combination with NIR-GECO (Fig. 4H)<sup>21</sup>. We attribute the apparent lower magnitude of the CoChR-induced transients primarily to slower Ca<sup>2+</sup> re-uptake in a more developmentally immature heart<sup>37</sup>, driving a higher baseline between transients. These results demonstrated that simultaneous expression of FR-GECO1 and blue light-

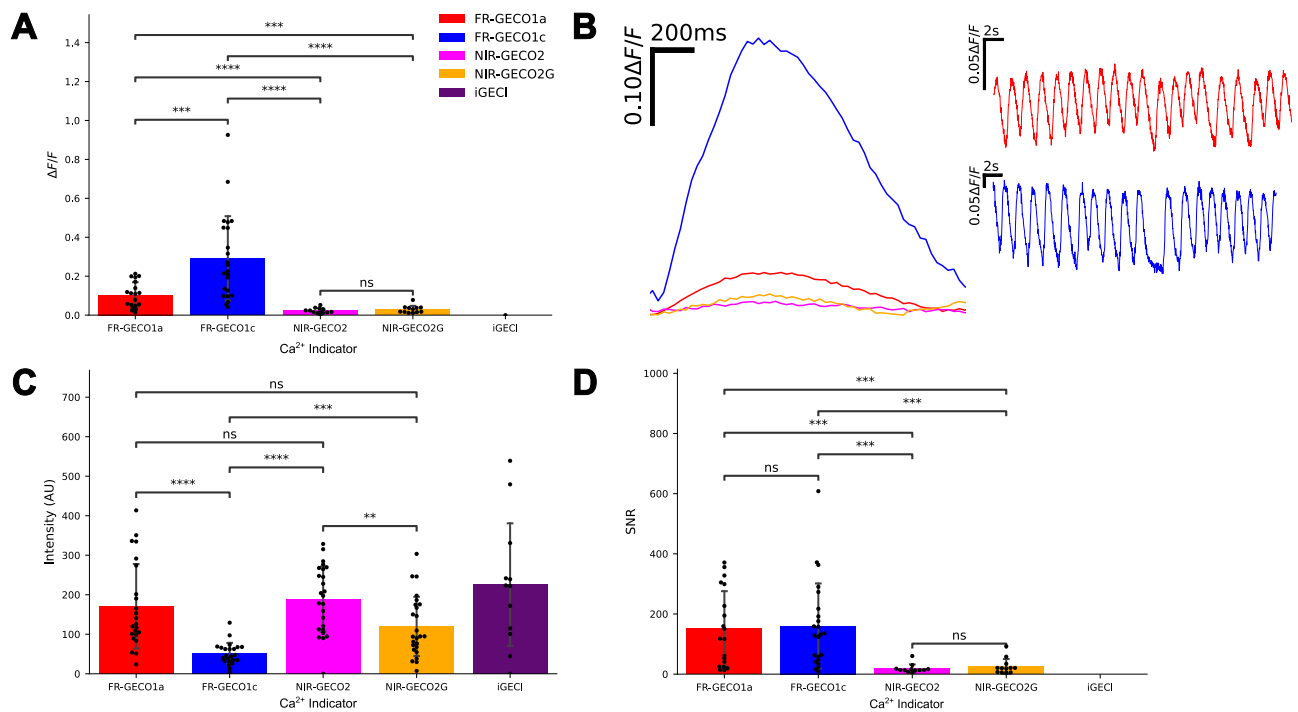


**Fig. 3 | Comparison between FR-GECO1 and near-infrared GECIs in the hearts of embryonic zebrafish in vivo**<sup>20–22</sup>. Fluorescence responses (**A**), average intensities (AU arbitrary units) (**C**), and SNRs (**D**) of FR-GECO1a, FR-GECO1c, NIR-GECO2, NIR-GECO2G, and iGECI. **B** Average of 5 spontaneous heartbeats from representative traces for each sensor (left) and representative traces (right) of FR-GECO1a and FR-GECO1c. Colors are consistent with other panels and iGECI was omitted for **A** and **B** since no Ca<sup>2+</sup>-dependent change in fluorescence was observed. **A–D**  $n = 23$  embryos for FR-GECO1a, 23 embryos for FR-GECO1c, 25 embryos for NIR-GECO2, 25 embryos for NIR-GECO2G, and 12 embryos for iGECI. Error bars are standard deviation. Statistical comparisons were performed using two-sided Welch's *t*-test with Benjamini–Hochberg multiple test correction (Shapiro–Wilk test for normality

$p > 0.5$  for all groups); n.s. not significant, \*\*\*  $p < 0.001$ , \*\*\*\*  $p < 0.0001$ . Exact *p* values are: **A** FR-GECO1a vs. FR-GECO1c  $p = 8.526 \times 10^{-4}$ , FR-GECO1a vs. NIR-GECO2  $p = 1.321 \times 10^{-5}$ , FR-GECO1a vs. NIR-GECO2G  $p = 8.468 \times 10^{-6}$ , FR-GECO1c vs. NIR-GECO2  $p = 1.7 \times 10^{-5}$ , FR-GECO1c vs. NIR-GECO2G  $p = 1.594 \times 10^{-5}$ , NIR-GECO2 vs. NIR-GECO2G  $p = 0.8796$ ; **C** FR-GECO1a vs. FR-GECO1c  $p = 2.474 \times 10^{-5}$ , FR-GECO1a vs. NIR-GECO2  $p = 0.3249$ , FR-GECO1a vs. NIR-GECO2G  $p = 7.260 \times 10^{-2}$ , FR-GECO1c vs. NIR-GECO2  $p = 6.933 \times 10^{-10}$ , FR-GECO1c vs. NIR-GECO2G  $p = 1.71 \times 10^{-4}$ , NIR-GECO2 vs. NIR-GECO2G  $p = 8.399 \times 10^{-4}$ ; **D** FR-GECO1a vs. FR-GECO1c  $p = 0.1057$ , FR-GECO1a vs. NIR-GECO2  $p = 2.227 \times 10^{-4}$ , FR-GECO1a vs. NIR-GECO2G  $p = 2.761 \times 10^{-4}$ , FR-GECO1c vs. NIR-GECO2  $p = 5.785 \times 10^{-5}$ , FR-GECO1c vs. NIR-GECO2G  $p = 6.629 \times 10^{-5}$ , NIR-GECO2 vs. NIR-GECO2G  $p = 0.6697$ . Source data are provided in a Source Data file.

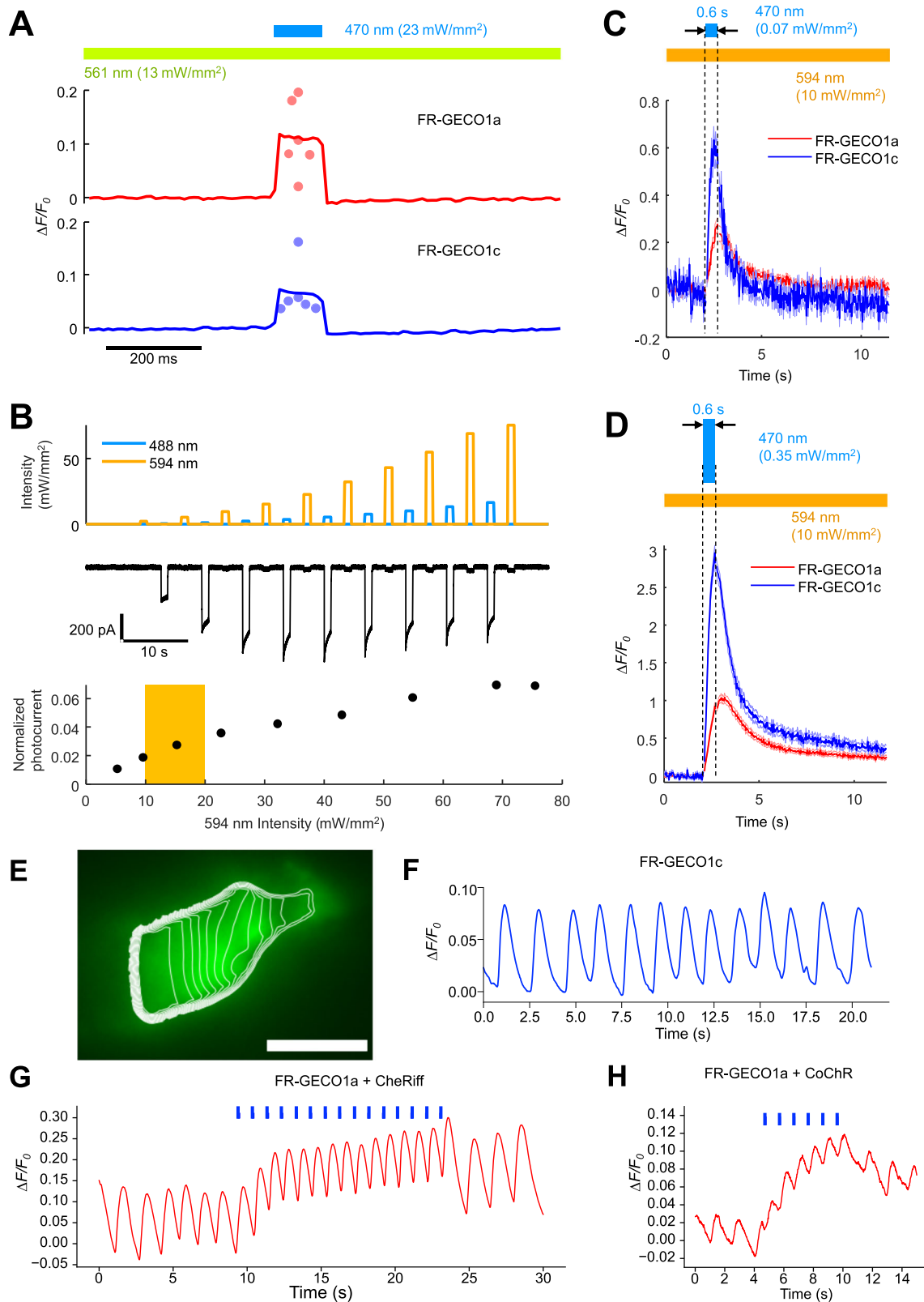
activated channelrhodopsins enables all-optical cardiac pacing and imaging of zebrafish embryonic hearts during development. More broadly, these results show that FR-GECO1a and 1c are compatible with blue light-activated channelrhodopsins for an optopatch approach to manipulating and imaging cells in culture or in vivo.

## Discussion

GFP- and RFP-based GECIs have been extensively engineered and are widely used for imaging cell signaling and neural activity in mammalian tissue in vivo. However, there remains a need for high-performance GECIs with more red-shifted wavelengths, such as indicators with wavelengths in the far-red or near-infrared range. Indicators with longer excitation and emission wavelengths enable deeper tissue imaging, which may be useful for imaging neural activity in subcortical structures, for example. They are also associated with less phototoxicity and less autofluorescence. Crucially, red-shifted indicators are also generally preferable to blue-shifted indicators as they provide better spectral separation from green indicators and commonly used optogenetic actuation tools such as channelrhodopsins, which allow for the manipulation and control of cells of interest. Here, we have reported the engineering and characterization of FR-GECO1a,c, two far-red fluorescent GECIs that are analogous to the GCaMP series of GECIs. Our initial efforts to engineer a far-red Ca<sup>2+</sup> indicator using other RFP scaffolds were unsuccessful, likely due to these scaffolds' oligomerization tendencies. On the other hand, mKelly2 is reported to be a true monomeric far-red FP, a property that likely helps to explain our success at using it as a scaffold to develop far-red fluorescent GECIs.

Both FR-GECO1 variants are bright relative to other red GECIs under 2P excitation. Their optimal 2P Ca<sup>2+</sup>-dependent  $\Delta F/F_0$  occurs between 1050 and 1200 nm, overlapping with the range of common tunable 2P lasers such as titanium-sapphire lasers which typically range from 650 to 1100 nm. Previous study has demonstrated that multi-photon excitation at longer wavelengths around 1200–1400 nm or 1600–1800 nm effectively provides optimal tissue imaging depths when considering both tissue scattering and water absorption<sup>38</sup>. When excited at 1200 nm, FR-GECO1a and FR-GECO1c, in their Ca<sup>2+</sup>-saturated states, have very high 2P brightness. At this wavelength, their brightness is comparable to commonly used bright far-red FPs, such as mKate2, tdKatushka2, and mNeptune<sup>39</sup>. Both indicators are much brighter upon 2P excitation at 1200 nm than any of the red GECIs characterized so far<sup>29</sup> (Supplementary Table 3), suggesting that the far-red mKelly2 scaffold may be more promising than the existing red FP scaffolds for the development of bright fluorescent sensors for 2P excitation.

In addition to greater depth penetration afforded by 2P microscopy, an important driving force for the development of red-shifted indicators is their better compatibility with existing blue-light activatable optogenetic tools. However, one concern is that some red GECIs exhibit transient fluorescence increases (photoactivation) when illuminated with blue light<sup>16</sup>, complicating their use in optogenetics. Through detailed photophysical characterization of FR-GECO1 photoactivation both in vitro and in cells, we have demonstrated that FR-GECO1 transiently photoactivates and recovers to baseline on the millisecond timescale. This fast rise and decay suggest that the photoactivation behavior of FR-GECOs, while not desirable, could still be



easily distinguished from action potential-evoked GECI Ca<sup>2+</sup> fluorescence changes, which typically happen on a timescale in the order of seconds due to the response kinetics of GECIs<sup>16,18,40</sup>. The spectral orthogonality and minimal crosstalk enabled us to combine FR-GECO1 with blue-light activated channelrhodopsins (CheRiff or CoChR) to create Ca<sup>2+</sup> optopatch for the all-optical stimulation and recording of excitable cells. Previously reported pairings of CheRiff/jRCaMP1b and

eTsChR/jRGECO1a were validated in cultured cells and acute tissue slices, respectively<sup>41,42</sup>. In this work, we further validated the Ca<sup>2+</sup> optopatch construct in vivo in the hearts of embryonic zebrafish.

In addition to the unique spectral profile, the FR-GECO1 series offers other advantages relative to other green, red, and NIR GECIs. FR-GECO1c exhibits a larger Ca<sup>2+</sup>-dependent  $\Delta F/F_0$  in vitro than most other red GECIs, such as K-GECO1, XCaMP-R and R-GECO1<sup>17,18,24</sup>. The use of

**Fig. 4 | Ca<sup>2+</sup> optopatch for all-optical electrophysiology in cultured neurons and in zebrafish embryonic heart in vivo.** **A** Average fluorescence trace of cultured rat hippocampal neurons expressing FR-GECO1a or 1c via transient transfection, under constant 561 nm illumination (13 mW/mm<sup>2</sup>) and 100 ms flash of 470 nm LED illumination (23 mW/mm<sup>2</sup>). Time-average of fluorescence increase induced by 470 nm illumination for each neuron was quantified and shown in red (FR-GECO1a) or blue (FR-GECO1c) dots ( $n = 6$  for both FR-GECO1a and 1c). **B** HEK293T cells transiently transfected with CheRiff were illuminated by alternating pulses of 488 nm and 594 nm light of increasing intensities (top). Photocurrents were measured under a voltage clamp at  $-65$  mV (middle). Photocurrents at 594 nm were then normalized to the maximum photocurrent induced by excitation with 488 nm (bottom). Typical light intensities used for optopatch experiments are highlighted in orange ( $n = 3$  cells). Average fluorescence traces of cultured rat hippocampal neurons expressing FR-GECO1a (or 1c)-P2A-CheRiff-

eGFP-Kv2.1 (AAV transduction) under constant 594 nm illumination (10 mW/mm<sup>2</sup>) and 470 nm optical stimulation for 0.6 s at 0.07 mW/mm<sup>2</sup> (**C**) or 0.35 mW/mm<sup>2</sup> (**D**) ( $n = 45$  neurons for FR-GECO1a;  $n = 37$  neurons for FR-GECO1c). Blue light crosstalk during the stimulation epochs (dotted lines) has been subtracted from the traces. Error bands represent S.E.M. **E** Isochronal map of calcium wave in an embryonic zebrafish linear heart tube (LHT) at 24 h post-fertilization (hpf). The map was calculated from a spike-triggered average ( $n = 12$  beats). Each isochron is 50 ms, propagating from left to right. Cardiac marker Nkx2.5:ZsYellow marked in green. Scale bar 50  $\mu$ m. **F** Mean FR-GECO1c  $\Delta F/F_0$  of the LHT in (**E**). Simultaneous pacing and measurement of Ca<sup>2+</sup> dynamics in the LHT using FR-GECO1a combined with optical stimulation at 1 Hz using CheRiff (**G**) and CoChR (**H**). FR-GECOs were imaged using constant 594 nm illumination at 24–290 mW/mm<sup>2</sup>. Channelrhodopsin was excited using 488 nm light at 24 mW/mm<sup>2</sup> (25 ms pulse for CoChR, 75 ms pulse for CheRiff). All images were acquired at 33 Hz. Source data are provided in a Source Data file.

ckkap peptide provides FR-GECO1a and FR-GECO1c with high affinities for Ca<sup>2+</sup> ( $K_d < 100$  nM), as well as large fluorescence changes and fast response times for detection of small numbers of action potentials, comparable to other ckkap-based GECIs such as K-GECO1 and the XCaMP series, and RS20-based indicators such as R-GECO1, and the GCaMP and RCaMP1 series<sup>17,18,24,33,43</sup>. The high sensitivity of FR-GECO1c is likely due to its lower Ca<sup>2+</sup>-free state fluorescence, larger Ca<sup>2+</sup>-dependent  $\Delta F/F_0$ , and optimal affinity towards Ca<sup>2+</sup>. Neurons typically have a basal intracellular [Ca<sup>2+</sup>] of 50 to 100 nM that can increase to 1 to 10  $\mu$ M upon stimulation<sup>44,45</sup>. FR-GECO1c's affinity ( $K_d = 83$  nM) is positioned in the ideal range to detect small and large changes in Ca<sup>2+</sup>. Indeed, the affinities of FR-GECO1 are comparable to sensitive variants of the late-generation GCaMP series<sup>43,46</sup>. Relative to NIR-GECO variants<sup>20,21</sup>, the FR-GECO1a,c variants are not as red-shifted but are brighter per molecule and have a direct (as opposed to inverse) response to Ca<sup>2+</sup>. Indicators with a direct response to their ligands are generally favored over indicators with an inverse response due to a better SNR owing to lower background fluorescence. In addition, FR-GECO1c offers better sensitivity and faster kinetics than NIR-GECO2 in neuronal activity detection<sup>21</sup>.

As first-generation GECIs, FR-GECO1a and FR-GECO1c both have the potential for further improvements. A general trend among FPs is that hypsochromic shifts in peak wavelengths are accompanied by reductions in quantum yield, thus limiting the brightness of available far-red and near-infrared FPs. Future versions of FR-GECO should be optimized for improved brightness to further facilitate imaging in vivo and even faster kinetics. Our pH titrations revealed that both FR-GECO1 variants have a significantly more basic  $pK_a$  than mKelly2 and so they do not exhibit their maximum brightness under physiological conditions. Accordingly, engineering variants with lower  $pK_a$  values may lead to improved brightness for imaging in tissue. Additionally, FR-GECO1a,c are the only non-biliverdin-binding GECIs that can be excited by the widely used red helium-neon lasers ( $\sim 633$  nm). Yet, due to the misalignment between the excitation peak (596 nm) and the laser wavelength, the excitation is only  $\sim 12.5\%$  of the possible maximum. Further red-shifted FR-GECO1a,c variants with better compatibility with helium-neon lasers could be another important future direction. FR-GECO1a and FR-GECO1c show substantial differences in performance, attributable to a single mutation, Tyr35Thr, at the interface of the FP and the CaM/ckkap domains. To obtain insight into the mechanisms of these biosensors, and the impact of the Tyr35Thr mutation, an experimentally-determined molecular structure of FR-GECO1 will likely be required. Such a structure could further our understanding of the mechanisms underpinning the performance FR-GECO1 and, consequently, serve to guide the development of improved generations of the FR-GECO series.

In summary, we have developed the FR-GECO series of far-red GECIs that expands the spectral palette of available GECIs that utilize archetypical (i.e., non-biliverdin-binding) FPs. Although only the first iteration, FR-GECO1a,c have good brightness, high affinities for Ca<sup>2+</sup>,

and very good sensitivity for neuronal activity detection. We have also successfully shown that FR-GECO1a,c can be used in conjunction with optogenetic actuators in all-optical studies. For these reasons, we are certain that FR-GECO1a,c are valuable additions to the GECI toolkit. Moreover, we anticipate that the cpmKelly2 scaffold of FR-GECO1 can serve as a template for engineering FP-based far-red indicators for ligands other than Ca<sup>2+</sup>.

## Methods

### Ethics statement

This research complies with all relevant ethical regulations. Procedures for preparation of primary neurons at Université Laval were approved by the Animal Ethics Committee and were performed according to Canadian Biosafety Guidelines in a Containment Level 2 certified lab. Procedures at Janelia Research Campus were approved by the Institutional Animal Care and Use Committee (IACUC) and the Institutional Biosafety Committee (IBC). All vertebrate experiments at Harvard University were approved by the Institutional Animal Care and Use Committee of Harvard University or the Harvard Medical Area Standing Committee on Animals. Procedures in the United States conform to the National Institutes of Health (NIH) Guide for the Care and Use of Laboratory Animals.

### General

Synthetic DNA oligonucleotides and double-stranded fragments (gBlocks) were sourced from Integrated DNA Technologies. CloneAmp HiFi PCR Premix (Takara Bio USA, Inc., 639298) and Q5 polymerase (New England Biolabs, M0491L) were used for high fidelity polymerase chain reactions (PCRs). Random mutagenesis PCRs were performed with Taq polymerase (Thermo Fisher Scientific, EP0406). PCR products were purified by preparative agarose gel electrophoresis and extracted with GeneJET Gel Extraction Kit (Thermo Fisher Scientific, K0692). Restriction enzymes and T4 DNA ligase (E0011) were purchased from Thermo Fisher Scientific and used according to the manufacturer's recommended protocols. Digested PCR products were extracted with the GeneJET Gel Extraction Kit before ligation. In-Fusion HD (Takara Bio USA, Inc., 639650) was used for assembly reactions. Plasmid DNA extractions were performed with GeneJET Plasmid Miniprep Kits (Thermo Fisher Scientific, K0503). Sanger sequencing reactions were performed by the Molecular Biology Services Unit at the University of Alberta. Fluorescence measurements were performed on a Safire<sup>2</sup> plate reader (Tecan), while absorbance measurements were collected on a DU-800 UV-Visible Spectrophotometer (Beckman).

### Protein engineering

**Starting template construction.** Double-stranded DNA encoding for K-GECO1<sup>17</sup>, with its circularly permuted (cp) FP replaced with cpmKelly2<sup>12</sup>, was commercially synthesized with overlapping sequences with pBAD/HisB (Invitrogen, V43001) in the 5' and 3' directions to facilitate insertion between the *Xho*I and *Hind*III sites. This fragment

was then assembled into pBAD/HisB vector digested with XhoI (Thermo Fisher Scientific, FD0694) and HindIII (Thermo Fisher Scientific, FD0504), and the assembly reaction was used to transform electrocompetent DH10B *E. coli* (Invitrogen, 18290015 and 12033015) prior to overnight incubation on Lennox Broth (LB; Fisher Scientific, BP1427-500) agar plates supplemented with 400 µg/mL ampicillin (Fisher Scientific, FLBP17605) and 0.02% (w/v) L-arabinose (Alfa Aesar, AAA1192130) at 37 °C. Plasmids were isolated from single colonies grown in 4 mL liquid LB cultures with 100 µg/mL ampicillin, and sequenced by Sanger sequencing.

**Plasmids for mammalian expression.** Genes encoding FR-GECO1a and FR-GECO1c were amplified by high-fidelity PCR using primers that add vector homologous sequences to the 5' and 3' end and assembled into linearized pcDNA3.1/Puro-CAG-ASAP1 to replace the gene encoding for ASAP1 (Addgene plasmid #52519, a gift from Michael Lin)<sup>47</sup>.

**Library construction.** To generate random mutagenesis libraries, mutations were introduced into the construct by error-prone PCR amplification with Taq polymerase in the presence of MnCl<sub>2</sub> (varies, up to 0.15 mM; Fisher Scientific, M87-100) and a 1:5 ratio of dATP and dGTP to dCTP and dTTP (Thermo Scientific, R0181). The purified PCR product was then assembled with an XhoI and HindIII-digested pBAD/HisB vector. Site-directed mutagenesis libraries were generated by PCR amplification with high fidelity polymerases and primers carrying the codons for the desired mutations followed by DpnI (Thermo Fisher Scientific, FD1703 and FD1704) digestion. The NNK codon was used for complete randomization. For mutations at just one position, amplification was performed with the CloneAmp HiFi PCR Premix, while libraries with mutations at multiple locations were generated by QuikChange Lightning Multi Site-Directed Mutagenesis Kit (Agilent Technologies, 200531).

**Library screening.** DH10B *E. coli* were transformed with DNA encoding the library and cultured on LB agar plates supplemented with ampicillin and L-arabinose, as described earlier. The *E. coli* colonies expressing the library were then screened on the plate based on fluorescence intensity using a custom imaging system described previously<sup>48</sup>. Briefly, this imaging system illuminates a Petri dish with light from a Lambda LS 175 W xenon arc lamp (Sutter Instruments) that has passed through an excitation filter (Chroma, ET560/40×) in a filter wheel (Lambda 10-3 from Sutter Instruments). Fluorescence is viewed either by eye through tinted goggles (Forensics Source), or using a CCD camera (QImaging) connected to a personal computer. Colonies displaying the highest fluorescence intensity were then cultured in 4 mL liquid LB with ampicillin and arabinose overnight at 37 °C. Proteins were then extracted from cells using B-PER (Thermo Fisher Scientific, 78248) and subjected to a secondary screen by measuring their fluorescence intensities in Ca<sup>2+</sup>-free (30 mM 3-(N-morpholino)propanesulfonic acid (MOPS; Thermo Fisher Scientific, A17214-22), 100 mM KCl (Sigma Aldrich, 529552-250GM), 10 mM ethylene glycol-bis(β-aminoethyl ether)-N,N,N',N'-tetraacetic acid (EGTA, pH 7.2; MP Biochemicals, ICN1948238), and Ca<sup>2+</sup> buffers (30 mM MOPS, 100 mM KCl, 10 mM Ca-EGTA, pH 7.2) to determine their Ca<sup>2+</sup>-dependent ΔF/F<sub>0</sub>. Plasmids for variants showing the largest Ca<sup>2+</sup>-dependent ΔF/F<sub>0</sub> and highest fluorescence intensities were extracted, sequenced, and used as the template(s) for the next round of evolution.

### In vitro characterization

**Protein expression and purification.** Electrocompetent DH10B *E. coli* were transformed with the pBAD/HisB plasmid carrying the gene encoding the protein of interest and grown on solid media. Single colonies from the transformed bacteria were then used to inoculate 4 mL of a starter culture supplemented with ampicillin and L-arabinose

that was then shaken at 225 rpm in 37 °C overnight. The starter culture was added to 500 mL of LB with 100 µg/mL ampicillin and the culture was shaken at 37 °C. After 4 h, 0.02% L-arabinose is added to induce expression, and the culture is shaken for another 4 h at 37 °C before harvesting the bacteria by centrifugation. Bacteria were then resuspended in 1× TBS (50 mM Tris-HCl, 150 mM NaCl, pH 7.5; Tris base from Fisher Scientific, BP152-5; NaCl from Fisher Scientific, BP3581), and lysed by sonication. The lysate was clarified by centrifugation and the cleared lysate was incubated with Ni-NTA resin (G Biosciences, 786-408) for at least 1 h. Resin bound to protein was washed with TBS wash buffer (1× TBS with 20 mM imidazole, pH 8.0; imidazole from Thermo Scientific, 396741000), followed by elution with TBS elution buffer (1× TBS with 250 mM imidazole, pH 7.8). The purified protein was then left at room temperature overnight to facilitate protein folding and chromophore maturation before concentrating and buffer exchanging into 1× TBS using 10 kDa centrifugal filter units (Millipore Sigma, UFC801024 and UFC 901024). Unless noted otherwise, all steps were carried out at 4 °C or on ice.

**Brightness, affinity, and pH-sensitivity measurement.** Effective ECs of FR-GECO variants were measured using the alkali denaturation method<sup>26</sup>. Briefly, purified protein for each FR-GECO variant was diluted in NaOH, Ca<sup>2+</sup>-free (30 mM MOPS, 100 mM KCl, 10 mM EGTA, pH 7.2), and Ca<sup>2+</sup> buffer (30 mM MOPS, 100 mM KCl, 10 mM Ca-EGTA, pH 7.2), and the absorption spectrum for each sample was collected. Because the same amount of protein was used for each set of measurements for each protein, the concentration of protein present in each sample can be calculated according to Beer's Law and the previously reported EC of 44,000 for the absorbance peak around 450 nm, which corresponds to the denatured tyrosine-based chromophore<sup>26,49</sup>. Further application of Beer's Law with the calculated concentration for each variant yields the EC in the Ca<sup>2+</sup>-bound and Ca<sup>2+</sup>-free states. Measurements were performed in triplicate and the results were averaged. Determination of QY was performed according to previously established protocols using mKelly2 as the standard<sup>12,24,48</sup>. For each protein, a series of diluted samples were prepared in Ca<sup>2+</sup>-free and Ca<sup>2+</sup> buffer from the samples used for extinction coefficient measurements such that the peak absorbance was equal to, or less than, 0.05. For each dilution series, the emission spectra were collected from 590 to 750 nm with an excitation wavelength of 570 nm. The total fluorescence intensities for each dilution were integrated, plotted against the absorbance, and the slope of each line (*m*) was calculated. Quantum yields were then calculated using the published quantum yield for mKelly2 (0.18)<sup>12</sup> and according to the equation:

$$\Phi_{\text{protein}} = \Phi_{\text{standard}} \times \frac{m_{\text{protein}}}{m_{\text{standard}}} \quad (1)$$

Buffers for the K<sub>d</sub> determination, with free [Ca<sup>2+</sup>] ranging from zero to 39 µM, were prepared by mixing appropriate volumes of Ca<sup>2+</sup>-free and Ca<sup>2+</sup> buffers<sup>50</sup>. Purified FR-GECO variants were diluted in these buffers and the fluorescence intensities of the protein in each solution were measured in triplicate. The readings were plotted against the free Ca<sup>2+</sup> concentration on a logarithmic scale, and the data fitted to the Hill equation for the K<sub>d</sub> and apparent Hill coefficient. Aliquots of a buffer containing 30 mM trisodium citrate and 30 mM borax (sodium borate) were adjusted using HCl or NaOH so that their pH ranged from 3 to 11. Concentrated protein, as well as 1 µL of either 200 mM EGTA or CaCl<sub>2</sub> for the Ca<sup>2+</sup>-free and Ca<sup>2+</sup> conditions, respectively, were then diluted in these buffers for a total volume of 100 µL. The fluorescence intensities were measured in triplicate, and the readings were plotted against pH. Due to the ionization events at pH 5 to 6, only the data for pH 6.5 to 11 were fitted to the Hill equation for the pK<sub>a</sub>.

**In vitro kinetics measurement.** Rapid kinetic measurements of FR-GECO1a and FR-GECO1c in purified protein were made using an Applied Photophysics SX-20 Stopped-Flow Reaction Analyzer using fluorescence detection. The dead time of the instrument was 1.1 ms. The excitation wavelength used was 625 nm with 2 nm bandwidth and emitted light was collected at 690 nm through a 10 mm path at room temperature. For  $k_{\text{off}}$  measurements, 2  $\mu\text{M}$  of each FR-GECO1a and FR-GECO1c proteins in 1 mM  $\text{Ca}^{2+}$  (30 mM MOPS, 100 mM KCl, pH 7.2) were rapidly mixed at 1:1 ratio with 100 mM of EGTA (30 mM MOPS, 100 mM KCl, pH 7.2) at room temperature. Measurements were taken for five replicates.  $k_{\text{off}}$  values were determined by fitting a single exponential dissociation curve to the signal decay with units of  $\text{s}^{-1}$ , using Prism GraphPad. For  $k_{\text{on}}$ , both variants, buffered in 30 mM MOPS and 100 mM KCl (pH = 7.2), were rapidly mixed at 1:1 ratio with varying concentrations of  $\text{Ca}^{2+}$  produced by reciprocal dilutions of 10 mM EGTA and 10 mM CaEGTA by using the Calcium Calibration Buffer Kit (Thermo Fisher Scientific, C3008MP). The slope of  $k_{\text{obs}}$  was used to determine the  $k_{\text{on}}$  rate in the units of  $\text{s}^{-1}\text{M}^{-1}$ . The tau values for both on and off rates were calculated as the reciprocal of the  $k_{\text{on}}$  and  $k_{\text{off}}$  rates, respectively. Two replicates were used for each  $\text{Ca}^{2+}$  concentration.

**Photoactivation measurement.** Microdroplets of FR-GECO1a and FR-GECO1c in purified protein in either  $\text{Ca}^{2+}$  or  $\text{Ca}^{2+}$ -free buffer (pH 7.2) were prepared using octanol (Sigma-Aldrich). The prepared sample was sandwiched between pre-silanized coverglass and coverslip (Sigma-Aldrich). Using a widefield microscope each droplet was continuously illuminated with a 561 nm laser for 120 s. 488 nm laser was used for photoactivation while the 561 nm laser was on. The 488 nm laser was on for 50 ms with the shutters switching on at various frequencies (0.2, 1, or 2 Hz).

**2P characterization.** Experimental setup for 2P spectral measurements includes a tunable femtosecond laser InSight DeepSee Dual (Spectra Physics) coupled with a photon-counting spectrofluorometer PCI (ISS)<sup>29,51</sup>. The 2P fluorescence excitation (2PE) spectra were measured by automatically stepping laser wavelength and recording total fluorescence intensity at each step. A combination of filters, including FF01-770/SP, FF01-680/SP (both Semrock), and FGL630 long-pass (Thorlabs) was used in the left emission channel of the PCI spectrofluorometer to eliminate scattered laser light. To scale the 2P excitation spectra, we use a parameter called 2P molecular brightness  $F_2(\lambda)$ . This parameter depends on fractional contributions to 2P brightness of the anionic and neutral forms at excitation wavelength  $\lambda$  and can be presented as follows:

$$F_2(\lambda) = \rho_A \varphi_A \sigma_{2,A}(\lambda) + \rho_N \varphi_N \sigma_{2,N}(\lambda) \quad (2)$$

where  $\varphi$  is the fluorescence quantum yield of form  $A$  or  $N$ , and  $\sigma_2$  is the 2P absorption cross-section. Since we collect fluorescence spectrum through an FGL630 long-pass filter, technically  $\varphi_N$  only comprises a part of fluorescence originating from anionic deprotonated chromophore that appears after the excited-state proton transfer from initially excited neutral form. To obtain the 2P excitation spectrum in units of molecular brightness, we independently measured  $\rho_A$ ,  $\varphi_A$ , and  $\sigma_{2,A}(\lambda)$  of the anionic form for both FR-GECO1a,c in  $\text{Ca}^{2+}$ -free and  $\text{Ca}^{2+}$ -saturated states and normalized the unscaled 2P spectrum to the product  $\rho_A \varphi_A \sigma_{2,A}(\lambda)$ . The cross-section  $\sigma_{2,A}(\lambda)$  was measured at the wavelength where the contribution of the neutral form is negligible ( $\lambda = 1064$  nm). This measurement was performed using Rhodamine B (Exciton, 06101) in alkaline ethanol as a reference standard. Its cross-section was measured relative to Rhodamine 6G (Sigma-Aldrich, 252441) in ethanol (with the average  $\langle \sigma_{2,\text{RhB}} / \sigma_{2,\text{Rh6G}} \rangle = 1.072 \pm 0.017$ ). Using this number together with the Rhodamine 6G cross-section in ethanol ( $\sigma_{2,\text{Rh6G}}$ ) obtained after averaging of seven independent measurements<sup>51</sup>:  $\langle \sigma_{2,\text{Rh6G}} \rangle = 12.4 \pm 2.6$  GM, the cross-section of

Rhodamine B in ethanol at 1064 nm was calculated  $\sigma_{2,\text{RhB}} = 13.3 \pm 2.8$  GM and used as a reference. In a modified version of previously reported method<sup>51</sup>, a total (without monochromator) 2P excited (at 1064 nm) fluorescence signals  $I$  as a function of laser power  $P$  were collected for both the sample and reference solutions (solutions were held in  $3 \times 3$  mm cuvettes (Starna) with a maximum optical density less than 0.1). The fluorescence was collected at  $90^\circ$  to excitation laser beam through FF01-770/SP, FGL630 Longpass, and long wave pass 561 (Edge Basic<sup>TM</sup>, Semrock) filters, using the left emission channel of a PCI spectrofluorometer working in a photon counting mode. The power dependences of fluorescence were fit to a quadratic function  $I = aP^2$ , from which the coefficients  $a_S$  and  $a_R$  were obtained for the sample (index S) and reference (index R) solutions, respectively. Second, the 1P excited fluorescence signals were measured for the same samples and in the same registration conditions. In this case, strongly attenuated radiation of a 561 nm line of a Sapphire 561-50 CW CDRH (Coherent) laser was used for excitation. The fluorescence power dependences for the sample and reference were measured and fit to a linear function:  $I = bP$ , from which the coefficients  $b_S$  and  $b_R$  were obtained. The 2P absorption cross-section was then calculated as follows:

$$\sigma_{2,S}(\lambda_2) = \frac{a_S b_R \varepsilon_S(\lambda_1)}{a_R b_S \varepsilon_R(\lambda_1)} \sigma_{2,R}(\lambda_2) \quad (3)$$

Here,  $\lambda_1$  is the wavelength used for 1P excitation (561 nm),  $\lambda_2$  is the wavelength used for 2P excitation (1064 nm),  $\varepsilon_{R,S}(\lambda_1)$  are the corresponding extinction coefficients, measured at  $\lambda_1$ . (In contrast to the one-photon characterization section, we define extinction coefficient ( $\varepsilon_S$ ) here to be of a particular, anionic, form. It relates to the previously defined extinction coefficient, e.g. shown in Table 1, as follows:  $\varepsilon_S = \varepsilon(\rho_A)$ ) This approach allows us to automatically correct for the laser beam properties (pulse duration and spatial intensity distribution), fluorescence collection efficiencies for 1P and 2P modes, PMT spectral sensitivity, differences in QYs and concentrations between S and R solutions. The molecular brightness of the anionic form was then calculated as a product  $F_2 = \rho_A \varphi_A \sigma_{2,A}(\lambda_m)$  with the 2P cross-section taken at spectral maximum,  $\lambda_m$ , for both states of the indicator. The QYs, ECs, and fractional concentrations were all measured independently. Finally, the 2P excitation spectra were scaled to the calculated  $F_2(1064$  nm) values.

## Imaging in cultured cells

**Imaging in HeLa cells.** The genes coding FR-GECO1a and FR-GECO1c were inserted into the pcDNA3.1 vector (Thermo Fisher Scientific, V79020) between the *XhoI* and *HindIII* restriction sites. The cells were cultured in Dulbecco's Modified Eagle Medium (Nakalai Tesque, 08456-65) supplemented with 10% fetal bovine serum (Sigma-Aldrich, F7524-500ML) and 1% penicillin-streptomycin (Nakalai Tesque, 09367-34). HeLa cells ( $\sim 10^4$ , ATCC, CCL-2) were seeded into 35-mm glass-bottom (collagen coated) cell-culture dishes (Iwaki, 3911-035) with 200  $\mu\text{L}$  opti-MEM (Thermo Fisher Scientific, 31985-070). Cells were transfected with the pcDNA-FR-GECO variants plasmid (2  $\mu\text{g}$ ) using 4  $\mu\text{L}$  polyethylenimine (Polysciences, 24765-1, 1 mg polyethylenimine diluted in 1 mL ultrapure water). Transfected cells were imaged three days after transfection using a IX83 wide-field fluorescence microscopy (Olympus) equipped with a pE-300 LED light source (CoolLED), a 40 $\times$  objective lens (numerical aperture = 1.3; oil), an ImagEM X2 EM-CCD camera (Hamamatsu), Cellsens software (Olympus), and a STR stage incubator (Tokai Hit). The filter sets for imaging were 545/20 nm excitation, 645-nm dclp dichroic mirror, and 678/65 nm emission. For imaging of  $\text{Ca}^{2+}$ -dependent fluorescence, the cells were washed twice with Hank's balanced salt solution with  $\text{Ca}^{2+}$  (HBSS(+); Nakalai Tesque, 09735-75), and the buffer was exchanged to 1 mL HBSS(+) supplemented with 10 mM HEPES (Nakalai Tesque,

17557-94) and incubated at 37 °C. Images were acquired every 5 s with an exposure time of 100 ms. After 1 min of imaging, histamine (Wako, 087-03533, 50 μM final concentration) was added. Imaging continued for 11 min, and then cells were washed twice with HBSS without Ca<sup>2+</sup> (HBSS(-)) (Nakalai Tesque, 17461-05), and 1 mL of HBSS(-) was added. After 1 min, EGTA/ionomycin (2.5 mM/1.5 μM final concentration) were added to fully deplete Ca<sup>2+</sup>. Once a steady fluorescence intensity was reached, the dish was washed twice more and supplemented with HBSS(-). Ca<sup>2+</sup>/ionomycin (5 mM/1.5 μM final concentration) was then immediately added to saturate the indicator.

**Imaging of spontaneous activity in cultured neurons.** Primary rat cortical neurons were prepared and maintained by the CERVO Brain Research Centre's Neuronal Culture Platform as previously described<sup>52,53</sup>. Briefly, neonatal rats were sacrificed and their cortices were dissected and dissociated with papain (Worthington, LS003126). Dissociated neurons were plated on 12 mm PDL-laminin coated glass coverslips and cultured in neurobasal media (Gibco, 21103049) supplemented with B-27 (Gibco, 17504044), GlutaMax (Gibco, 35050-061), FBS (Hyclone, SH30071.03), and penicillin/streptomycin (Gibco, 15140031), with Ara-C (Sigma Aldrich, C-1768) added 5 days after plating. Neurons were then fed twice a week by replacement of half the growth medium with serum- and Ara-C-free growth medium. At 5 days in vitro (DIV), neurons were transfected with adeno-associated viruses (AAVs) encoding FR-GECO1-WPRE (2.4 × 10<sup>10</sup> GC/well) under the control of either the CAG or human synapsin promoter and imaging was performed on DIV 15. Prior to imaging, neurons were washed thrice in HBSS supplemented with 10 mM HEPES (pH 7.4). Images were acquired on a Zeiss Observer Z.1 equipped with a 20× objective (NA = 0.4, LD Plan-Neofluar 20×, Zeiss), a CCD camera (AxioCam 503 m), HXP 120 V light source, and filter set 00 (BP 530-585 nm excitation, FT 600 nm dichroic mirror, and LP 615 nm emission; Zeiss). Images were acquired for 20 min with 5 s intervals, 1.5 s exposure time and 2 × 2 binning. Images were first aligned to correct for drift as needed, and baseline corrected prior to analysis in ImageJ and plotting on Prism GraphPad.

**Imaging of cultured neurons with electrical stimulation.** Primary rat hippocampal and cortical neurons were prepared and maintained as described previously<sup>46</sup>. Briefly, neonatal rat pups (Charles River Laboratory) were euthanized, and hippocampal and cortical tissues were isolated and dissociated using papain (Worthington) in 10 mM HEPES (pH 7.4) in Hanks' Balanced Salt Solution, incubating at 37 °C for 30 min. The cell suspension was triturated, filtered (40 μm), and electroporated with 400 ng of plasmid DNA in nucleofection solution (Lonza). Neurons were plated at 1 × 10<sup>5</sup> cells per well in poly-D-lysine-coated, 96-well glass-bottom plates (MatTek) with a 4:1 ratio of NbActiv4 (BrainBits) to plating medium (28 mM glucose, 2.4 mM NaHCO<sub>3</sub>, 100 μg/mL transferrin, 25 μg/mL insulin, 2 mM L-glutamine, 100 U/mL penicillin, 10 μg/mL streptomycin, and 10% FBS in MEM). On the following day, 190 μL of NbActiv4 medium was added to each well and plates were incubated at 37 °C with 5% CO<sub>2</sub> for 12–15 days before imaging.

Cultured neurons were transfected with an expression vector with hSyn1-NES-FR-GECO1-WPRE, where FR-GECO1 included the leader sequence of pBAD, using electroporation (Lonza Nucleofector) according to the manufacturer's instructions. Imaging and the corresponding analysis were performed as described previously<sup>46</sup>. Specifically, prior to the imaging session, transfected neurons were first washed thrice with imaging buffer (140 mM NaCl, 0.2 mM KCl, 30 mM glucose, 10 mM HEPES, pH 7.4), and treated with synaptic blockers (10 μM CNQX, 10 μM CPP, 10 μM gabazine, and 1 mM MCPG (Tocris Bioscience)). Neurons were imaged using an inverted Olympus IX81 microscope equipped with a 10× objective (NA = 0.4, UPlanSApo, Olympus), an EMCCD camera (Ixon Ultra DU897, Andor), a 565 nm LED for excitation (Cairn Research) and mCherry filter cubes (#49008,

Chroma). Neurons were stimulated at room temperature by field stimulation with a custom-built electrode. Trains of 3, 10 and 160 APs were stimulated and fluorescence images were acquired at 206 Hz throughout the stimulation session. Reference images were taken after stimulation to perform cell segmentation during analysis.

For image analysis, cell segmentation was performed using the Suite2P package in Python. Background fluorescence was subtracted from the images before calculating  $\Delta F/F_0$ . The  $\Delta F/F_0$  value for each segmented cell was determined by dividing the fluorescence intensity after stimulation by the baseline fluorescence ( $F_0$ ) and subtracting 1. Half-rise time and half-decay time were computed by fitting a one-phase exponential rise or decay curve on the fluorescence traces.

### Ca<sup>2+</sup> Optopatch

**Cell culture.** HEK293T cells (ATCC, CRL-3216) were grown at 37 °C, 5% CO<sub>2</sub>, in DMEM with 10% fetal bovine serum (Life Technologies, 10082-147) and 50 U/mL penicillin-streptomycin (Life Technologies, 15060-063). Cell confluency was maintained at <80% by splitting every 2-3 days using trypsin-EDTA (Life Technologies, 25300054). Cell passage numbers were maintained <15. Hippocampal neurons from postnatal day 0 (P0) rat pups were dissected and cultured at a density of 30,000–40,000 cells per cm<sup>2</sup> on a laminin (Fisher Scientific, 23-017-015) and poly-D-lysine (PDL, Sigma-Aldrich, P1024) coated glass-bottom dish (Cellvis, D35-14-1.5-N), using Brainphys Neuronal Medium (STEMCELL Technologies, 05792, 05794), following the manufacturer's protocols.

**DNA constructs.** A Kv2.1 soma-localization sequence was appended to the C terminus of CheRiff-eGFP<sup>54</sup> (Addgene plasmid #51693). To combine optogenetics with Ca<sup>2+</sup> imaging, soma-localized CheRiff-eGFP-Kv2.1 and FR-GECO1a (or 1c) were linked with a ribosomal skip sequence P2A and co-expressed from a single vector<sup>55</sup>. An AAV backbone for Cre-dependent expression under hSyn promoter (Addgene plasmid #126512) was linearized via restriction digestion with NheI (New England Biolabs, R3131S) and AscI (New England Biolabs, R0558S). The FR-GECO, P2A, and CheRiff-eGFP-Kv2.1 were cloned into the AAV backbone via Gibson assembly (New England Biolabs, E2611S) to obtain hSyn-DiO-FR-GECO1a(or 1c)-P2A-CheRiff-eGFP-Kv2.1.

**Imaging and electrophysiology.** Cell culture media were replaced by the imaging buffer, consisting of 125 mM NaCl, 2.5 mM KCl, 2.5 mM HEPES, 30 mM glucose, 1 mM MgCl<sub>2</sub>, 3 mM CaCl<sub>2</sub>, with a pH of 7.3 and osmolarity of 310 mOsm. For photocurrent measurement, HEK293T cells were transfected with FCK-CheRiff-eGFP (Addgene plasmid #51693) using TransIT-293 (Mirus, MIR2700). After two days, cells were plated on PDL-coated glass-bottom dishes at a density of ~100,000 cells/cm<sup>2</sup>. Cells were allowed to settle and adhere for 6 h prior to measurement. Borosilicate glass capillaries (WPI, 1B150F-4) were pulled to tip resistances of 5-10 MΩ, and filled with internal solution of 125 mM potassium gluconate, 8 mM NaCl, 0.6 mM MgCl<sub>2</sub>, 0.1 mM CaCl<sub>2</sub>, 1 mM EGTA, 10 mM HEPES, 4 mM Mg-ATP, 0.4 mM Na-GTP, adjusted to pH 7.3 and 295 mOsm with sucrose. For photocurrent measurement, HEK293T cells were voltage-clamped to -65 mV, then illuminated with alternating 1 s pulses of 488 nm (Coherent, Obis 1226419) and 594 nm laser light (Huber Photonics, 0594-04-01-0100-300) at intensities 1-17 and 0.5–75 mW/mm<sup>2</sup>, respectively. Current recordings were collected using MultiClamp 700B amplifier (Molecular Devices), filtered at 5 kHz with the amplifier's internal Bessel filter, and digitized at 10 kHz.

For photoswitching characterization, neurons were transfected with CAG-FR-GECO1a (or 1c) plasmid using Lipofectamine 2000 (Fisher Scientific, 11-668-027) on DIV 7-10, and imaged on DIV 14-18 using a custom microscope described previously<sup>42</sup>. For photoswitching measurements, neurons were continuously illuminated with 561 nm light (MPB Communications, F-04306-02), at 13 mW/mm<sup>2</sup> for 10 s, while 100 ms flashes

of 470 nm LED (Thorlabs, M470L3) light at 1 Hz (23 mW/mm<sup>2</sup>) were used to induce photoswitching. Fluorescence emission was collected using a 10× objective (Olympus, XLPan N 10× SVMP, NA 0.6), filtered through a band-pass filter (Chroma, ET600/50 m), and imaged onto a scientific CMOS camera (Hamamatsu, Orca Flash 4.0) at 100 Hz.

For all-optical neurophysiology measurement, cultured rat hippocampal neurons at DIV 3–4 were transduced using AAVs encoding hSyn-Cre and hSyn-DIO-FR-GECO1a(or 1c)-P2A-CheRiff-eGFP-Kv2.1. Cells were imaged on DIV 14–19. Neurons were illuminated with continuous 594 nm light (Hubner Photonics, Cobolt Mambo™ 100 mW) at 10 mW/mm<sup>2</sup>, while a 600 ms pulse of 470 nm light at 0.07 or 0.35 mW/mm<sup>2</sup> was used to stimulate CheRiff. Fluorescence emission was collected using a wide field 2× objective (Olympus, MVPLAPO 2XC, NA 0.5), filtered through a bandpass filter (Semrock, FF02-641-75), and imaged at 30 Hz.

**Data analysis.** To determine the crosstalk of 594 nm light into CheRiff activation, the 594 nm photocurrents were normalized by the maximum (saturating) 488 nm photocurrent. The 488 nm photocurrents were calculated by averaging the photocurrent during the last 100 ms of a 1 s long stimulus. The 594 nm photocurrents were calculated by averaging the photocurrent during the last 500 ms of a 1 s long stimulus.

For optical crosstalk and all-optical neurophysiology analysis, fluorescence traces were extracted by averaging the movie pixels in manually defined regions of interest containing single neurons. To correct for the fluorescence background of the imaging buffer, pixels surrounding the neuron were averaged then subtracted from the fluorescence traces. The mean optical crosstalk response was calculated by averaging five trials of blue light stimulation in cells expressing FR-GECO1a or 1c and not expressing a channelrhodopsin. To calculate the optical crosstalk artifact ( $\Delta F/F_0$ ), we defined  $F_0$  as the mean fluorescence during the initial 100 ms of orange-only illumination, and  $\Delta F$  as the mean increase in fluorescence during the 100 ms blue light stimulus. To calculate fluorescence traces during the all-optical neurophysiology experiments, optical crosstalk was first corrected by subtracting the fluorescence increase at the onset of the blue light stimuli. This procedure relied on the fact that optical crosstalk was effectively instantaneous, while optogenetically induced Ca<sup>2+</sup> increases took several tens of milliseconds to develop.  $F_0$  was calculated by the 2 s average of the baseline fluorescence and  $\Delta F$  was calculated as the increase in fluorescence above the baseline.

### In vivo imaging in embryonic zebrafish

**GECI comparisons in embryonic zebrafish.** *TgBAC(-36nkx2.5:ZsYellow)* embryos were injected with 20 fmol of GECI mRNA, in addition to 25 pg of  $\alpha$ -bungarotoxin mRNA (synthesized using pmtb-t7-alpha-bungarotoxin (Addgene plasmid #69542) and the mMESSAGE mMACHINE SP6 Transcription Kit (Thermo Fisher Scientific, AM1340)) and 4 ng of *tnnt2a* morpholino (Gene Tools). 30× Danieau buffer was prepared according to the following recipe: 1740 mM NaCl, 21 mM KCl, 12 mM MgSO<sub>4</sub>·7H<sub>2</sub>O, 18 mM Ca(NO<sub>3</sub>)<sub>2</sub>, 150 mM HEPES buffer. 25  $\mu$ M biliverdin (Sigma, 30891) or vehicle (1% DMSO in 0.3× Danieau buffer, pH 7.4) was added to embryos at 14 hpf. Embryos were raised to 24–30 hpf and dechorionated using 1 mg/mL Pronase (Sigma, 53702). All sensors were imaged for 30 s at 40 Hz frame-rate with 23 mW/mm<sup>2</sup> illumination intensity, using an Olympus XLPLN25XWMP2 objective (25×, water immersion). FR-GECO1 variants were excited using a Cobolt Mambo 594 nm laser and emission fluorescence was collected through a 640/57 nm filter. Near-infrared sensors were excited using an Opto-Engine MLL-FN-639 laser and emission fluorescence was collected through a 665 nm long-pass filter (Chroma, ET665lp). Cardiac tissue was identified by the Otsu thresholding technique applied to an image of ZsYellow fluorescence. The point with the highest GECI intensity within the cardiac tissue was selected as the centroid of a circle with radius 3  $\mu$ m for extraction of signal. Mean intensity and  $\Delta F/F$  for each

signal trace were calculated after subtracting mean intensity of control embryos without GECI injection and performing correction for photobleaching by subtracting the local minimum value in a trace over a moving window of two seconds as described previously<sup>34</sup>. SNR was calculated by taking the ratio of the mean power in the fluorescence dynamics between 0.1 Hz and 1.5 Hz over the mean power outside of this frequency band. Embryos with SNR < 5 were discarded. Statistical comparisons were performed using Welch's *t*-test with Benjamini-Hochberg multiple test correction (Shapiro-Wilk test for normality  $p > 0.5$  for all groups).

**All-optical electrophysiology of embryonic zebrafish.** Zebrafish *Danio rerio* were raised at 28 °C. The transgenic line *TgBAC(-36nkx2.5:ZsYellow)* (AB background) was used to mark the embryonic heart<sup>56</sup>. Open reading frames of FR-GECOs and channelrhodopsins, CheRiff and CoChR, were cloned into the pMTB plasmid backbone<sup>57</sup> and capped mRNA was synthesized using the mMESSAGE mMACHINE™ SP6 Transcription Kit (Thermo Fisher Scientific). 100 pg of FR-GECO mRNA was injected into fertilized eggs at the 1-cell stage, in addition to 25 pg of  $\alpha$ -bungarotoxin mRNA<sup>58</sup> to arrest tail twitches and 4 ng of *tnnt2a* morpholino oligonucleotide (CATGTTTGCTCTGATCTGACACGCA, Gene Tools) to arrest heart motion<sup>59</sup>. 25 pg of CoChR-GFP and 50 pg of CheRiff-GFP RNA were included in the injection mix in the respective experiments. Embryos were raised to 20 hpf and dechorionated using 1 mg/mL Pronase (Sigma). FR-GECOs were imaged using a Cobolt Mambo 594 nm laser (100 mW) and channelrhodopsins were stimulated using a Coherent Obis 488 nm laser (100 mW). The blue light was targeted to the heart using a digital micromirror device to avoid spurious stimulation of ChR in other tissues. Images were recorded using an Olympus XLPLN25XWMP2 objective (25×, water immersion) and a Hamamatsu Orca Flash sCMOS camera. Segmentation was performed by thresholding an *nkx2.5:ZsYellow* image and manually adjusting it.  $\Delta F/F$  traces were obtained by subtracting background, performing a linear photobleach correction, and taking the 10th percentile of fluorescence intensity as the baseline. Spike-triggered averages were obtained by performing peak detection on the  $\Delta F/F$  trace and averaging across samples within a window flanking the peak. Spatial isochrons were calculated by identifying the time to half maximum of the spike-triggered average at every image pixel and spatially smoothing with a mean filter.

### Statistics and reproducibility

Details of the exact statistical tests used, and sample sizes used, are provided in the figure legends. Replication information for all data reported in this study is stated in figure legends. All repetitions were deemed successful. No statistical method was used to predetermine sample size. No data were excluded from the analyses. The experiments were not randomized. The Investigators were not blinded to allocation during experiments and outcome assessment.

### Reporting summary

Further information on research design is available in the Nature Portfolio Reporting Summary linked to this article.

### Data availability

Source data are provided with this paper. Plasmid constructs encoding FR-GECO1a and FR-GECO1c with a CAG promoter are available through Addgene (Plasmid IDs #163681 and #163682, respectively). The full DNA and protein sequences of FR-GECO1a and FR-GECO1c are provided in Supplementary Table 4. The previously reported crystal structure for FusionRed which was used as a reference for numbering mutations, is available under PDB ID 6UIA. Source data are provided with this paper.

## References

1. Tromberg, B. J. et al. Non-invasive in vivo characterization of breast tumors using photon migration spectroscopy. *Neoplasia* **2**, 26–40 (2000).
2. Lyons, S. K., Patrick, P. S. & Brindle, K. M. Imaging mouse cancer models in vivo using reporter transgenes. *Cold Spring Harb. Protoc.* **2013**, 685–699 (2013).
3. Abbyad, P., Childs, W., Shi, X. & Boxer, S. G. Dynamic Stokes shift in green fluorescent protein variants. *Proc. Natl Acad. Sci. USA* **104**, 20189–20194 (2007).
4. Lin, M. Z. et al. Autofluorescent proteins with excitation in the optical window for intravital imaging in mammals. *Chem. Biol.* **16**, 1169–1179 (2009).
5. Strack, R. L. et al. A rapidly maturing far-red derivative of DsRed-Express2 for whole-cell labeling. *Biochemistry* **48**, 8279–8281 (2009).
6. Chu, J. et al. Non-invasive intravital imaging of cellular differentiation with a bright red-excitable fluorescent protein. *Nat. Methods* **11**, 572–578 (2014).
7. Shen, Y., Lai, T. & Campbell, R. E. Red fluorescent proteins (RFPs) and RFP-based biosensors for neuronal imaging applications. *Neurophotonics* **2**, 031203 (2015).
8. Hense, A. et al. Monomeric Garnet, a far-red fluorescent protein for live-cell STED imaging. *Sci. Rep.* **5**, 18006 (2015).
9. Bajar, B. T. et al. Fluorescent indicators for simultaneous reporting of all four cell cycle phases. *Nat. Methods* **13**, 993–996 (2016).
10. Shen, Y., Chen, Y., Wu, J., Shaner, N. C. & Campbell, R. E. Engineering of mCherry variants with long Stokes shift, red-shifted fluorescence, and low cytotoxicity. *PLoS ONE* **12**, e0171257 (2017).
11. Matela, G. et al. A far-red emitting fluorescent marker protein, mGarnet2, for microscopy and STED nanoscopy. *Chem. Commun.* **53**, 979–982 (2017).
12. Wannier, T. M. et al. Monomerization of far-red fluorescent proteins. *Proc. Natl Acad. Sci. USA* **115**, E11294–E11301 (2018).
13. Yu, D. et al. A naturally monomeric infrared fluorescent protein for protein labeling in vivo. *Nat. Methods* **12**, 763–765 (2015).
14. Rodriguez, E. A. et al. A far-red fluorescent protein evolved from a cyanobacterial phycobiliprotein. *Nat. Methods* **13**, 763–769 (2016).
15. Shemetov, A. A., Oliinyk, O. S. & Verkhusha, V. V. How to increase brightness of near-infrared fluorescent proteins in mammalian cells. *Cell Chem. Biol.* **24**, 758–766.e3 (2017).
16. Dana, H. et al. Sensitive red protein calcium indicators for imaging neural activity. *Elife* **5**, e12727 (2016).
17. Shen, Y. et al. A genetically encoded Ca<sup>2+</sup> indicator based on circularly permuted sea anemone red fluorescent protein eqFP578. *BMC Biol.* **16**, 9 (2018).
18. Inoue, M. et al. Rational engineering of XCaMPs, a multicolor GECI suite for in vivo imaging of complex brain circuit dynamics. *Cell* **177**, 1346–1360. e24 (2019).
19. Wu, J. et al. Improved orange and red Ca<sup>2+</sup> indicators and photo-physical considerations for optogenetic applications. *ACS Chem. Neurosci.* **4**, 963–972 (2013).
20. Qian, Y. et al. A genetically encoded near-infrared fluorescent calcium ion indicator. *Nat. Methods* **16**, 171–174 (2019).
21. Qian, Y. et al. Improved genetically encoded near-infrared fluorescent calcium ion indicators for in vivo imaging. *PLoS Biol.* **18**, e3000965 (2020).
22. Shemetov, A. A. et al. A near-infrared genetically encoded calcium indicator for in vivo imaging. *Nat. Biotechnol.* **39**, 368–377 (2021).
23. Shcherbakova, D. M. Near-infrared and far-red genetically encoded indicators of neuronal activity. *J. Neurosci. Methods* **362**, 109314 (2021).
24. Zhao, Y. et al. An expanded palette of genetically encoded Ca<sup>2+</sup> indicators. *Science* **333**, 1888–1891 (2011).
25. Carlson, H. J. & Campbell, R. E. Mutational analysis of a red fluorescent protein-based calcium ion indicator. *Sensors* **13**, 11507–11521 (2013).
26. Cranfill, P. J. et al. Quantitative assessment of fluorescent proteins. *Nat. Methods* **13**, 557–562 (2016).
27. Muslinkina, L. et al. Two independent routes of post-translational chemistry in fluorescent protein FusionRed. *Int. J. Biol. Macromol.* **155**, 551–559 (2020).
28. Nasu, Y., Shen, Y., Kramer, L. & Campbell, R. E. Structure- and mechanism-guided design of single fluorescent protein-based biosensors. *Nat. Chem. Biol.* **17**, 509–518 (2021).
29. Molina, R. S. et al. Understanding the fluorescence change in red genetically encoded calcium ion indicators. *Biophys. J.* **116**, 1873–1886 (2019).
30. Inoue, M. et al. Rational design of a high-affinity, fast, red calcium indicator R-CaMP2. *Nat. Methods* **12**, 64–70 (2015).
31. Kerruth, S., Coates, C., Dürst, C. D., Oertner, T. G. & Török, K. The kinetic mechanisms of fast-decay red-fluorescent genetically encoded calcium indicators. *J. Biol. Chem.* **294**, 3934–3946 (2019).
32. Carlson, H. J. & Campbell, R. E. Circularly permuted red fluorescent proteins and calcium ion indicators based on mCherry. *Protein Eng. Des. Sel.* **26**, 763–772 (2013).
33. Akerboom, J. et al. Genetically encoded calcium indicators for multi-color neural activity imaging and combination with optogenetics. *Front. Mol. Neurosci.* **6**, 2 (2013).
34. Hochbaum, D. R. et al. All-optical electrophysiology in mammalian neurons using engineered microbial rhodopsins. *Nat. Methods* **11**, 825–833 (2014).
35. Arrenberg, A. B., Stainier, D. Y. R., Baier, H. & Huisken, J. Optogenetic control of cardiac function. *Science* **330**, 971–974 (2010).
36. Klapoetke, N. C. et al. Independent optical excitation of distinct neural populations. *Nat. Methods* **11**, 338–346 (2014).
37. Jia, B. Z., Qi, Y., Wong-Campos, J. D., Megason, S. G. & Cohen, A. E. A bioelectrical phase transition patterns the first vertebrate heartbeats. *Nature* **622**, 149–155 (2023).
38. Horton, N. G. et al. In vivo three-photon microscopy of subcortical structures within an intact mouse brain. *Nat. Photonics* **7**, 205–209 (2013).
39. Drobizhev, M., Makarov, N. S., Tillo, S. E., Hughes, T. E. & Rebane, A. Two-photon absorption properties of fluorescent proteins. *Nat. Methods* **8**, 393–399 (2011).
40. Chen, T.-W. et al. Ultrasensitive fluorescent proteins for imaging neuronal activity. *Nature* **499**, 295–300 (2013).
41. Afshar Saber, W., Gasparoli, F. M., Dirks, M. G., Gunn-Moore, F. J. & Antkowiak, M. All-optical assay to study biological neural networks. *Front. Neurosci.* **12**, 451 (2018).
42. Farhi, S. L. et al. Wide-area all-optical neurophysiology in acute brain slices. *J. Neurosci.* **39**, 4889–4908 (2019).
43. Dana, H. et al. High-performance calcium sensors for imaging activity in neuronal populations and microcompartments. *Nat. Methods* **16**, 649–657 (2019).
44. Berridge, M. J., Lipp, P. & Bootman, M. D. The versatility and universality of calcium signalling. *Nat. Rev. Mol. Cell Biol.* **1**, 11–21 (2000).
45. Grienberger, C. & Konnerth, A. Imaging calcium in neurons. *Neuron* **73**, 862–885 (2012).
46. Zhang, Y. et al. Fast and sensitive GCaMP calcium indicators for imaging neural populations. *Nature* **615**, 884–891 (2023).
47. St-Pierre, F. et al. High-fidelity optical reporting of neuronal electrical activity with an ultrafast fluorescent voltage sensor. *Nat. Neurosci.* **17**, 884–889 (2014).
48. Ai, H.-W., Baird, M. A., Shen, Y., Davidson, M. W. & Campbell, R. E. Engineering and characterizing monomeric fluorescent proteins for live-cell imaging applications. *Nat. Protoc.* **9**, 910–928 (2014).

49. Gross, L. A., Baird, G. S., Hoffman, R. C., Baldrige, K. K. & Tsien, R. Y. The structure of the chromophore within DsRed, a red fluorescent protein from coral. *Proc. Natl Acad. Sci. USA* **97**, 11990–11995 (2000).
50. Tsien, R. & Pozzan, T. Measurement of cytosolic free Ca<sup>2+</sup> with quin2. *Methods Enzymol.* **172**, 230–262 (1989).
51. Drobizhev, M., Molina, R. & Hughes, T. Characterizing the Two-photon Absorption Properties of Fluorescent Molecules in the 680–1300 nm Spectral Range. *BIO-PROTOCOL* **10**, e3498 (2020).
52. Nault, F. & De Koninck, P. Dissociated Hippocampal Cultures. in *Springer Protocols Handbooks* 137–159 (Humana Press, Totowa, NJ, 2009).
53. Wiesner, T. et al. Activity-dependent remodeling of synaptic protein organization revealed by high throughput analysis of STED nanoscopy images. *Front. Neural Circuits* **14**, 57 (2020).
54. Lim, S. T., Antonucci, D. E., Scannevin, R. H. & Trimmer, J. S. A novel targeting signal for proximal clustering of the Kv2.1 K<sup>+</sup> channel in hippocampal neurons. *Neuron* **25**, 385–397 (2000).
55. Kim, J. H. et al. High cleavage efficiency of a 2A peptide derived from porcine teschovirus-1 in human cell lines, zebrafish and mice. *PLoS ONE* **6**, e18556 (2011).
56. Zhou, Y. et al. Latent TGF- $\beta$  binding protein 3 identifies a second heart field in zebrafish. *Nature* **474**, 645–648 (2011).
57. Xiong, F. et al. Specified Neural Progenitors Sort to Form Sharp Domains after Noisy Shh Signaling. *Cell* **153**, 550–561 (2013).
58. Swinburne, I. A., Mosaliganti, K. R., Green, A. A. & Megason, S. G. Improved long-term imaging of embryos with genetically encoded  $\alpha$ -bungarotoxin. *PLoS ONE* **10**, e0134005 (2015).
59. Sehnert, A. J. et al. Cardiac troponin T is essential in sarcomere assembly and cardiac contractility. *Nat. Genet.* **31**, 106–110 (2002).

## Acknowledgements

We thank Saaya Hario, Dr. Fern Sha, Rosario Valenti, the Janelia Research Campus cell culture facility, and the University of Alberta Molecular Biology Services Unit, for technical assistance. Ronak Patel is a member of the Janelia Research Campus Tool Translation Team (T3); we thank the T3 for providing equipment access and technical support. We thank Dr. Timothy Wannier for sharing the mKelly sequences and the laboratory of Caroline and Geoffrey Burns (Boston Children's Hospital) for generously providing the TgBAC(-36nkx2.5:ZsYellow) transgenic zebrafish line. This work was supported by grants from the Natural Sciences and Engineering Research Council of Canada (NSERC; RGPIN-2018-04364 to R.E.C.), the Canadian Institutes of Health Research (CIHR; FS-154310 to R.E.C.), the Japan Society for the Promotion of Science (KIBAN(S) 19H05633 and KIBAN(A) 24H00489 to R.E.C.; KIBAN(B) 23K26794 to T.T.), the National Institutes of Health (NIH) BRAIN Initiative (1R01NS126102-01 to R.E.C.), and the Janelia Visiting Scientist Program (Janelia Research Campus, HHMI). We acknowledge NIH/NINDS BRAIN Initiative grant U24NS109107 (M.D.; Resource for Multiphoton Characterization of Genetically-Encoded Probes), NIH grants 1R01NS133755 (A.E.C.) and 1R01NS126043 (A.E.C.), and Chan Zuckerberg Dynamic Imaging grant 2023-321177 (A.E.C.).

## Author contributions

Y.S. and R.E.C. conceived the project. Y.S., R.D., and J.W. performed protein engineering. R.D., A.A., Y.Z., Y.S., M.D., R.S.M., A.S.A., and R.P. performed in vitro protein characterization. R.D., K.S., A.A., J.Z., D.R., J.P.H., and The GENIE Project Team performed cultured cell imaging and analysis. Y.Q. performed the Ca<sup>2+</sup> optopatch. B.Z.J. performed all-optical electrophysiology of embryonic zebrafish. Y.S., K.P., A.G.T., E.R.S., T.E.H., S.G.M., T.T., M.E.P., A.E.C., and R.E.C. supervised the research. Y.S., R.D., M.D., and R.E.C. wrote the paper. All authors read and approved the final paper.

## Competing interests

The authors declare no competing interests.

## Additional information

**Supplementary information** The online version contains supplementary material available at <https://doi.org/10.1038/s41467-025-58485-z>.

**Correspondence** and requests for materials should be addressed to Yi Shen or Robert E. Campbell.

**Peer review information** *Nature Communications* thanks Samuel Wang, and the other, anonymous, reviewer(s) for their contribution to the peer review of this work.

**Reprints and permissions information** is available at <http://www.nature.com/reprints>

**Publisher's note** Springer Nature remains neutral with regard to jurisdictional claims in published maps and institutional affiliations.

**Open Access** This article is licensed under a Creative Commons Attribution-NonCommercial-NoDerivatives 4.0 International License, which permits any non-commercial use, sharing, distribution and reproduction in any medium or format, as long as you give appropriate credit to the original author(s) and the source, provide a link to the Creative Commons licence, and indicate if you modified the licensed material. You do not have permission under this licence to share adapted material derived from this article or parts of it. The images or other third party material in this article are included in the article's Creative Commons licence, unless indicated otherwise in a credit line to the material. If material is not included in the article's Creative Commons licence and your intended use is not permitted by statutory regulation or exceeds the permitted use, you will need to obtain permission directly from the copyright holder. To view a copy of this licence, visit <http://creativecommons.org/licenses/by-nc-nd/4.0/>.

© The Author(s) 2025

---

## The GENIE Project Team

Jihong Zheng<sup>5</sup>, Daniel Reep<sup>5</sup>, Jeremy P. Hasseman<sup>5</sup>, Getahun Tsegaye<sup>5</sup>, Arthur Tsang<sup>5</sup> & Glenn C. Turner<sup>5</sup>